Modelling of Mechanical-Corrosion Interaction in Dapped-End Connections

Auteur : Léonard, Louise
Promoteur(s) : Mihaylov, Boyan
Faculté : Faculté des Sciences appliquées
Diplôme : Master en ingénieur civil des constructions, à finalité spécialisée en "civil engineering"
Année académique : 2022-2023
URI/URL : http://hdl.handle.net/2268.2/17871

Université de Liège
Faculté des Sciences Appliquées
Academic year 2022-2023

Modelling of Mechanical-Corrosion Interaction in Dapped-End Connections

Master thesis submitted in fulfillment of the requirements for the Master Degree in Civil Engineering

Louise Léonard

Promotor
Mihaylov Boyan

Jury members
Flawinne Sébastien
Courard Luc
Franssen Jean-Marc

Liège
June 2023

Acknowledgements

First of all, I would like to thank my promotor Boyan Mihaylov for all his help and advice throughout this master thesis. I would also like to thank his PhD student Sameera Hippola for his help.

I would also like to thank the members of the jury for their interest in this study and for taking the time to read my master thesis.

Finally, I want to thank all the authors and researchers without whom this work wouldn't have been possible.

Abstract

The aim of this master thesis is to model the behavior of reinforced concrete dapped-end beams subjected to the effects of corrosion. This type of connection is encountered in many reinforced concrete bridges and presents a concentration of stresses due to the abrupt reduction in cross-section. In addition, the infiltration of water and salts into the cracks can severely damage the structure and reduce the resistance of these elements.

The model used in this work is a kinematic-based model adapted to take account of the effects of corrosion. The model predicts the ultimate strength of connections as well as their crack width. The effects of corrosion modelled in this work are the degradation of steel's mechanical properties and the reduction of bond strength between the concrete and reinforcement due to corrosion.

Several models are proposed to take into account these two effects, and then compared in order to retain only one for each. The complete behavior of corroded reinforced concrete dapped-end beams is then studied, and the theoretical results are compared with experimental data gathered from scientific literature. Finally, the parameters that can influence the behavior of corroded half-joints are investigated.

The model predictions follow the expected reduction in strength due to the effects of corrosion, and a reduction in strength similar to that observed for less reinforced uncorroded specimens. However, more tests should be conducted on corroded dapped-end beams in order to conclude on the validity of the model.

The model presented in this work can be used as a basis for future studies, for example to model pitting corrosion more locally in the nib of the dapped-end.

Résumé

Ce travail de fin d'études a pour but de modéliser le comportement de l'extrémité de poutres en béton armé subissant une réduction de section et soumise aux effets de la corrosion. Ce type de connection est rencontré dans beaucoup de ponts en béton armé et présente une concentration de contraintes due à la réduction brusque de section. De plus, l'infiltration d'eau et des sels dans les fissures peuvent fortement endommager la structure et réduire la résistance de ces éléments.

Le modèle utilisé dans ce travail est un modèle basé sur la cinématique et adapté pour tenir compte des effets de la corrosion. Le modèle prédit la résistance ultime des connections ainsi que la largeur des fissures. Les effets de la corrosion modélisés dans ce travail sont la dégradation des propriétés mécaniques de l'acier ainsi que la réduction de l'adhérence à l'interface béton-renforcement due à la corrosion.

Plusieurs modèles sont proposés pour modéliser ces deux effets et ensuite comparés afin de n'en retenir qu'un pour chaque effet. Le comportement complet de l'extrémité de poutres en béton armé subissant une réduction de section et soumise aux effets de la corrosion est alors étudié et les résultats théoriques sont ensuite comparés aux données expérimentales récoltées dans des articles scientifiques. Enfin, les paramètres pouvant influencer le comportement d'extrémités de poutres à section réduite corrodées sont étudiés.

Les prédictions du modèle suivent la réduction de résistance attendue due aux effets de la corrosion, et une réduction de résistance semblable à celle observée pour des spécimens moins renforcés. Cependant, le nombre de tests sur des extrémités de poutres subissant une réduction de section corrodées est insuffisant pour vraiment conclure quant à la validité du modèle.

Le modèle présenté dans ce travail peut servir de base pour de futures études visant notamment à modéliser la corrosion par piqûre plus localement au niveau de la connection.

Contents

List of Figures

Chapter 1

Introduction

1.1 Context and motivation

Dapped-end beams or Gerber beams are very common in bridges as they are easy to build and make the structure isostatic. These kind of beams were introduced by the builder Heinrich Gottfried Gerber (1832–1912) of Nuremberg, Germany, to make a continuous structure isostatic by dividing it in several hinged girders, that can either be simply supported or resting on two cantilevered supports. The support system of such beams has a reduced area. The support, called a dapped-end connection or half-joint or Gerber saddle, is composed of a L-shaped ledge supporting an inverted ledge of a drop-in span (see Figure 1.1).

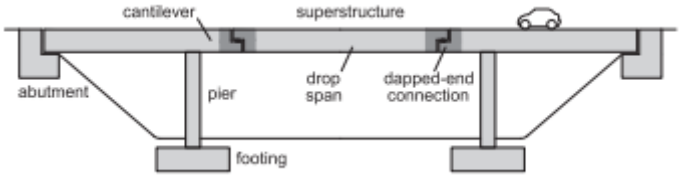

Figure 1.1: Typical bridge with dapped-end connections [30]

Compared to simply supported beams, the Gerber beam allows one to combine the advantages of continuous beams, as the structure allows the rotation of the joints in correspondence to the sections with no bending moment, which gives a bending moment distribution typical of continuous beams, to those of statically determined structures [11]. Another advantage is that it allows the use of precast beams, which simplifies the construction.

The reduction of section creates a stress concentration. This type of joint is designed as a D-region, that is a "disturbed" region, where Bernoulli's hypothesis is not valid, as opposed to B-regions. To design dapped-end connections, strut-and-tie models can be used [17] as well as FE models [33]. In this work, the model used is a kinematic-based model developed by Rajapakse et al. (2021) [30].

Gerber saddles pose problems of safety and durability as they are vulnerable to chloride attacks, causing corrosion of the reinforcement and degradation of the concrete. Rainwater and de-icing salts can percolate and stagnate at the location of the joint and trigger corrosion. Moreover, the geometry of these joints make them difficult to inspect and maintain[33]. The durability of those connections is an important subject, as a single half-joint's collapse might cause the failure of the entire structure as it is an isostatic system. It is therefore of interest to be able to model accurately the behavior of those structures after degradation.

Figure 1.2 shows a deteriorated dapped-end connection. As the reinforcement is corroded, the concrete also deteriorates (cracks, spalling) and the resistance of the structure is reduced.

Figure 1.2: Deteriorated dapped-end connection [30]

1.2 Objectives of the thesis

The purpose of this master thesis is to extend the kinematic-based model developed for the evaluation of dapped-end connections' behavior in order to account for the effects of corrosion. The effects implemented in the model are the reduction of the yield strength of reinforcing bars and the reduction of bond strength. This extended model would allow the prediction of the flexural strength of the connection as well as the opening of the main inclined crack.

1.3 Thesis outline

The following work is composed of six chapters and the bibliography.

Chapter 2 presents the literature review. The kinematic-based model developed by Rajapakse et al. (2021) is detailed as it will be the base of the corrosion model. Then this chapter explains what is corrosion and what are its causes. Finally, it reports the experimental data used for the corrosion models as well as the data of corroded dapped-ends.

Chapter 3 presents several models used to predict the stress-strain relationship of corroded bars and the reduction of bond strength due to corrosion.

Chapter 4 presents the comparison between the models from Chapter 3 in order to pick one model for stress-strain relationship and one for the reduction of bond strength to use in the remaining of the work. The predicted complete behavior of corroded dapped-ends is then presented and compared to experimental data.

Chapter 5 studies the effect of several parameters on the behavior of corroded dapped-ends.

Chapter 6 summarizes the conclusions that can be drawn from this study.

Chapter 2

Literature review

2.1 Kinematics-based model for flexural behavior of dapped-end connections

The model developed by Rajapakse et al. (2021) [30] predicts the peak capacity of dapped-end connections based on the crack along the re-entrant corner.

2.1.1 Kinematics

Dapped-end connections work mainly in flexure and cracks propagate from the re-entrant corner. The model considers a main crack, which separates the dapped-end into two rigid blocks that rotate with respect to each other about the tip of the crack. The crack is inclined by an angle θ from the horizontal axis that can be measured on site. The rotation of the two blocks causes large deformations in the compressive zone at the top of the member. The compression damage zone (designated as CDZ) that develops in this part is V-shaped and is bound by the top surface of the member and two planes inclined by an angle α from the horizontal axis. As there is no recommended value for this angle in the literature, it has been calibrated based on 47 tests from the literature. The resulting value is 50°.

The geometry of the CDZ can be fully defined by its depth d_{CDZ}. As can be seen in Figure 2.1, the strain profile has a constant value of $\epsilon_{CDZ} = -0.0035$ within the depth d_{CDZ} and transitions linearly from ϵ_{c0} to zero within the rest of the compression depth x. Therefore, d_{CDZ} can be evaluated as follows :

$$d_{CDZ} = (1 - \frac{\epsilon_{c0}}{\epsilon_{CDZ}})x \tag{2.1}$$

where x is the unknown of the model.

The relative rotation between the two rigid blocks ϕ can then be evaluated from Eq. 2.2 :

$$\phi = \frac{(2d_{CDZ}cot\alpha)\epsilon_{CDZ}}{x} \tag{2.2}$$

The relations for the displacements between the crack faces at the location of the reinforcement and in the different directions of the reinforcement also need to be evaluated. For a dapped-end with horizontal, vertical and diagonal reinforcement, the displacements are :

$$\begin{aligned} w_h &= \phi \times (l_{cr} sin\theta - c_h) \\ w_v &= \phi \times (l_{cr} cos\theta - c_v) \\ w_d &\approx \phi \times (l_{cr} - c_d) \end{aligned} \tag{2.3}$$

where c_h, c_v and c_d are respectively the horizontal, vertical and diagonal distances measured from the re-entrant corner of the connection to the respective reinforcement and l_{cr} is the length of the crack, which is equal to :

$$l_{cr} = \frac{h - x}{sin\theta} \tag{2.4}$$

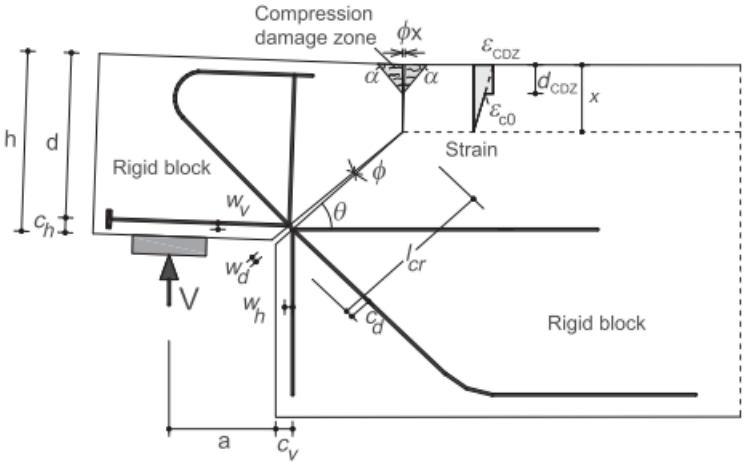

Figure 2.1: Kinematics of dapped-end connections governed by the widening of an inclined crack [30]

2.1.2 Evaluation of flexural strength

As said in the previous section, the depth of the compression zone x is the unknown of the model. It will be evaluated thanks to an iterative procedure, that verifies the equilibrium of the forces acting on a free body bound by the inclined crack. Those forces are shown in Figure 2.2 and include the external force H, the tension forces in the reinforcement and the compression forces in the concrete above the crack.

To start the procedure, it is necessary to estimate the value of x. It is recommended to take 20% of the effective depth of the section as a first estimation. From x and the value of θ, it is possible to determine the entire geometry of the kinematic model. The depth of the damage zone is calculated from Eq. 2.1, the angle of rotation ϕ from Eq. 2.2, and the crack displacements at the location of the horizontal, vertical and diagonal

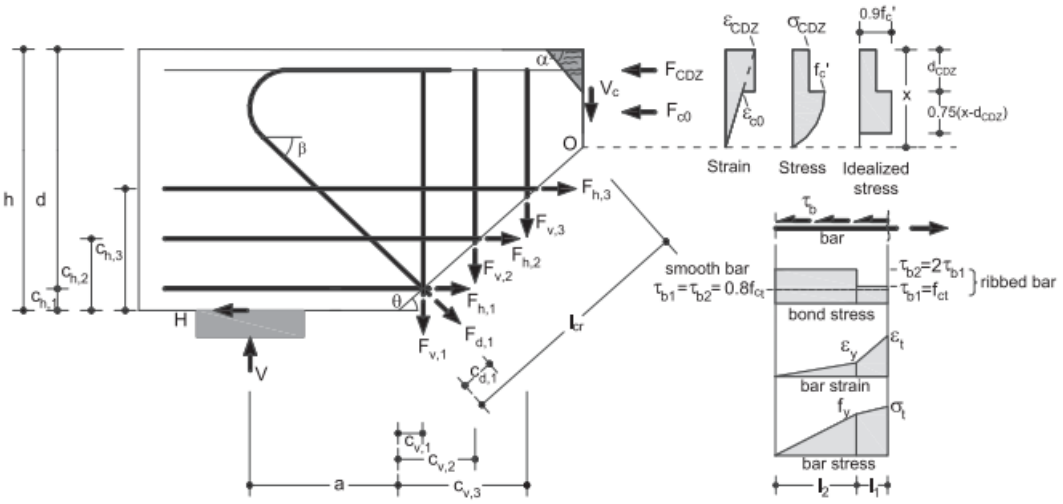

Figure 2.2: Forces acting on the free body diagram bound by the corner crack [30]

reinforcement from Eq. 2.3.

Once those parameters are calculated, the resisting forces in the compression zone can be computed. For this calculation, the strain and stress state are idealized as shown in Figure 2.2. The stress in the damage zone σ_{CDZ} corresponds to a strain $\epsilon_{CDZ} = -0.0035$ and is obtained by using the Popovics model [28] as extended by Collins et al. [12] as constitutive law for concrete under uniaxial compression. The stress state of the compression zone below is idealized by a rectangular stress block as in flexural calculations. The stress-strain relationship for the concrete is assumed to be parabolic in this zone and the stress-block factors have been evaluated for a maximum strain of ϵ_{c0}.

The resisting force in the damage zone F_{CDZ} is calculated from Eq. 2.5 :

$$F_{CDZ} = \sigma_{CDZ} d_{CDZ} b \tag{2.5}$$

where b is the width of the beam. The resisting force corresponding to the idealized block of the compression zone below the CDZ is given by Eq. 2.6 :

$$F_{c0} = (0.9 f_c')0.75(x - d_{CDZ})b \tag{2.6}$$

where f_c' is the concrete cylinder strength.

Now that the compression forces have been calculated, it is necessary to compute the tension forces in the dapped-end reinforcement. To do so, the tensile stresses σ_t that develop in the rebars are computed by using a mechanical model by Sigrist [34] for a given displacement in the inclined crack w. In this model, the reinforcement is analysed as being anchored by bond in the concrete blocks on each side of the crack. Two length are defined, dividing the anchorage length into two parts. The length l_1 near the crack is the length where the reinforcement yields and farther from the crack, the length l_2 is defined as the length where the reinforcement is elastic. These lengths are calculated from Eq. 2.7 and 2.8.

$$l_1 = max(\sigma_t - f_y, 0)\frac{d_b}{4\tau_{b1}} \tag{2.7}$$

$$l_2 = min(\sigma_t, f_y)\frac{d_b}{4\tau_{b2}} \tag{2.8}$$

The model assumes a constant bond stress between the concrete and the reinforcement in each zone and $\tau_{b2} = 2\tau_{b1}$, with $\tau_{b1} = f_{ct} = 0.3(f'_c)^{2/3}$ (MPa), the tensile strength of the concrete. If smooth bars are used, the bond stress is reduced to the constant value $\tau_{b1} = \tau_{b2} = 0.8f_{ct}$ (MPa). The assumption $\tau_{b1} = f_{ct}$ implies full bond strength since it corresponds to the pullout of ribbed reinforcement bars anchored in uncracked concrete under uniaxial loading. However, due to the presence of several cracks parallel to the corner crack and other effects, the bond strengh of the dapped-end is weaker than in the case of pullout from uncracked concrete. A bond strength reduction factor $k < 1$ is then introduced to represent this phenomenon [29]. The bond stress becomes $\tau_{b1} = kf_{ct}$. The reduction bond factor k is calculated from Eq. 2.9:

$$k = 0.41(\rho_{h,eff}d_{bh}/16)^{-0.44} \tag{2.9}$$

where $\rho_{h,eff}$ is the effective reinforcement ratio and d_{bh} is the bar diameter of the horizontal reinforcement in the dapped-end. The effective reinforcement ratio is calculated from Eq. 2.10 :

$$\rho_{h,eff} = \frac{\sum_{i=1}^{n} A_{sh,i}}{b(c_{h,1} + c_{h,n})} \times 100(\%) \tag{2.10}$$

where n is the number of layers of horizontal reinforcement. The numerator gives the total area of the reinforcement while the denominator gives the effective concrete area surrounding the bars. Quantities $c_{h,i}$ are the concrete cover of layer i of reinforcement.

Eq.2.11 gives the crack displacement considering the equilibrium of the bar :

$$w = 2\left[\frac{1}{2}\left(\epsilon_t + \frac{f_y}{E_s}\right)l_1 + \frac{1}{2}min\left(\epsilon_t, \frac{f_y}{E_s}\right)l_2\right] \tag{2.11}$$

where f_y is the yield strength of the bars, d_b is the bar diameter, E_s is the modulus of elasticity of steel, and ϵ_t is the strain in the reinforcement in the crack. This last component is expressed with stress σ_t by using a bi-linear stress-strain relationship for the steel with strain hardening. This relationship will be adapted to take into account the effects of corrosion in section 3.1. As the crack displacement is expressed as a function of ϵ_t, the stresses in the horizontal, vertical and diagonal reinforcement are evaluated by applying an iterative procedure.

Once the bar stresses and corresponding forces are calculated, the horizontal equilibrium of the free body illustrated in Figure 2.2 can be verified with Eq. 2.12 :

$$\sum_i F_{h,i} + \sum_i F_{d,i}cos\beta - H = F_{CDZ} + F_{c0} \tag{2.12}$$

with i the number of reinforcement layers, and β the inclination of the diagonal reinforcement. If the equilibrium is not achieved, the depth of the compression zone x is adapted and the procedure is repeated until satisfaction of the condition above. Once the condition is satisfied, the support shear at failure V_{pred} can be calculated, with the obtained x, by considering the moment equilibrium about the tip of the inclined crack :

$$\begin{aligned} V_{pred} &= \frac{1}{\alpha + l_{cr}cos\theta}\{\sum F_{h,i}(h - x - c_{h,i}) \\ &+ \sum F_{v,i}(l_{cr}cos\theta - c_{v,i}) + \sum F_{d,i}cos\beta sin\theta(l_{cr} - c_{d,i}) \\ &+ \sum F_{d,i}sin\beta cos\theta(l_{cr} - c_{d,i}) + 0.625F_{c0}(x - d_{CDZ}) \\ &+ F_{CDZ}(x - 0.5d_{CDZ}) - H(l_{cr}sin\theta)\} \end{aligned} \tag{2.13}$$

Figure 2.3 illustrates the iterative procedure described above.

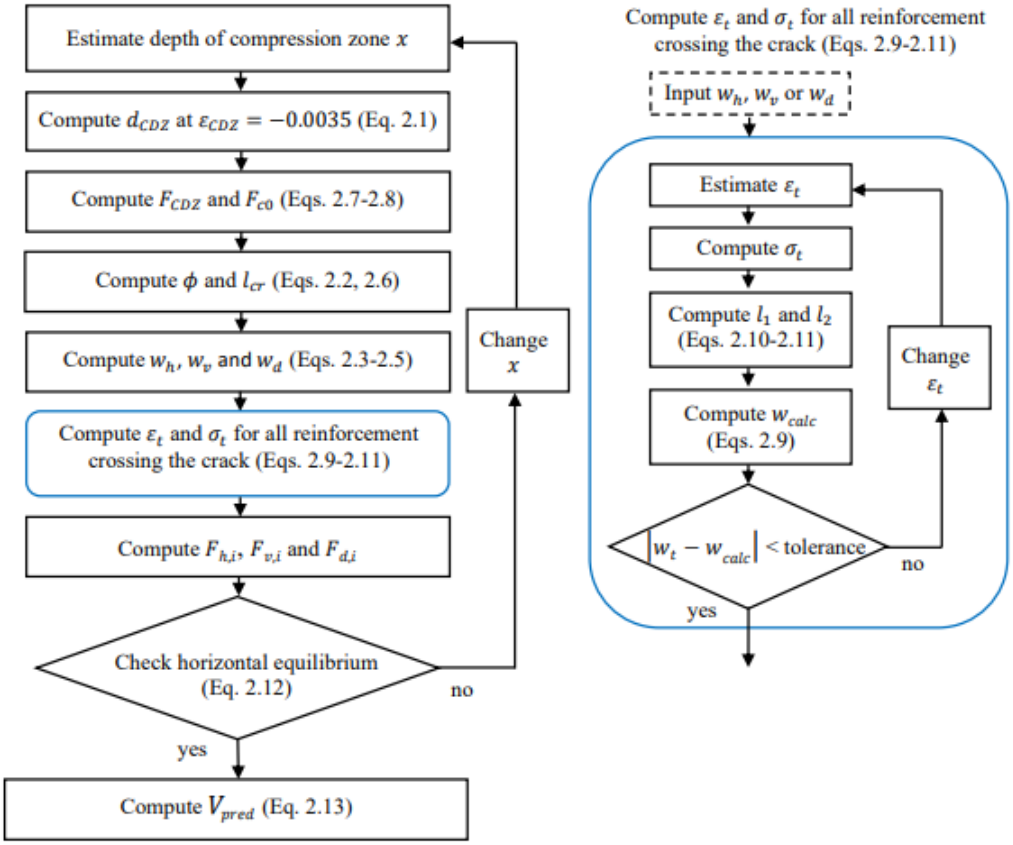

Figure 2.3: Flowchart of the iterative procedure [30]

2.2 Corrosion

Corrosion occurs when a difference in electrical potential along the steel in concrete allows the formation of an electrochemical cell. An anodic and a cathodic region form, the pore water in the hardened cement paste acting as an electrolyte to connect the two [26].

Concrete-embedded steel is in a passive state thanks to a thin film formed at the interface between steel and concrete [20]. The alkaline environment created by the hydrating cement guarantees the formation of the passivating layer [15]. Corrosion of concrete-embedded steel requires the destruction of this protective layer through depassivation. The most common factors initiating depassivation are the presence of depassivating agents, such as chlorides, in large enough amounts for passivating layers to be locally destroyed, or a decrease in the pH of the concrete below 8-9.5 due to carbonation [20]. Other factors can accelerate the rate of corrosion, such as water, an electrolyte or the presence of oxygen.

Figure 2.4: Corroded bars [1]

Corrosion impacts the reinforcement in itself (Figure 2.4) but also the concrete and the bond between both. Regarding the effects on the reinforcement, corrosion leads to loss of the steel section and degradation of the mechanical resistance as well as the ductility of the bars as will be developed in section 3.1. The products formed by the reaction of corrosion being more voluminous than the steel reinforcement, it increases the radial stresses, which leads to the deterioration of concrete through the formation of cracks, usually parallel to the reinforcement [26]. The degradation of the concrete matrix makes it easier for depassivating agents to get to the reinforcement, which in turn increases the corrosion rate [26]. Finally, the bond between concrete and the reinforcement is deteriorated by the corrosion as will be developed in section 3.2.

Signs of corrosion of reinforced concrete structures include rust spots, cracks in the concrete or spalling of the concrete cover [20].

2.2.1 Carbonation

Carbonation is the reaction between carbon dioxide present in the environment and the calcium hydroxide present in the cement paste, which produces calcium carbonate and water (2.14). This reaction lowers the pH of concrete to about 9, which leads to the breakage of the protective passivating layer and makes corrosion of the reinforcement possible [15]. Several factors can influence the reaction, such as the water-cement ratio, the quantity of cement and its type, the relative humidity, etc. Carbonation results in general corrosion.

$$CO_2 + H_2O + Ca(OH)_2 \longrightarrow CaCO_3 + H_2O \tag{2.14}$$

2.2.2 Chloride-induced corrosion

Chloride ions, when in presence of water and oxygen, destroy the passivating layer surrounding steel reinforcement [26]. For the chloride ions to trigger corrosion, the presence of crevices or some geometrical heterogeneity at the interface between steel and concrete is required as well as the presence of oxygen and water [20]. A relative humidity of 70-80% is optimum for the reaction to occur [26]. The pore system of the hardened cement paste will greatly influence corrosion. Chloride-induced corrosion is localized at a small anode, which leads to pitting of the steel [26]. Although chloride attack is started locally, it can lead to more widely-corroded zones with the formation of shallow pits as new corrosion points appear and propagate laterally [20].

Once the electrochemical cell is set up, the reactions are :

$$\begin{aligned} Fe^{2+} + 2Cl^- &\longrightarrow FeCl_2 \\ FeCl_2 + 2H_2O &\longrightarrow Fe(OH)_2 + 2HCl \end{aligned} \tag{2.15}$$

Chlorides can be found directly in the concrete mix through the use of contaminated aggregates or sea water or brackish water or even the use of admixtures containing chlorides [26]. Limits on the chloride content of concrete are prescribed to avoid any risk of chloride-induced corrosion. However they can ingress from outside. This can be caused by de-icing salts, sea water, or organic materials. In the specific context of dapped-end connections, chloride ingress is mostly found on the inner corners of the L-shaped ledge due to leakage through the expansion joint [16].

There is a certain period of time before chloride ions actually trigger corrosion of the reinforcement, called initiation period (Figure 2.5), and during which chloride ions and water diffuse into concrete until it reaches the necessary concentration (usually 0.2% for chlorides diffusing in concrete).

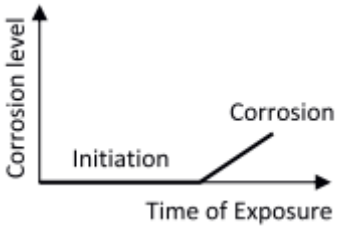

Figure 2.5: Initiation time[4]

2.2.3 Experimental data

In this section, data from the tests used to model the stress-strain relationship of corroded steel and the reduction of bond strength due to corrosion is presented. As it is assumed in this work that dapped-end connections are mainly affected by chloride-induced corrosion, the tests presented for the determination of stress-strain relationships of corroded bars are related only to pitting corrosion.

2.2.3.1 Tests by Imperatore et al. (2017) [21]

Imperatore et al. conducted tests on artificially corroded bare steel bars in the Laboratory of the University of Rome Tor Vergata. The corrosion on those specimen was uniform, similar to the effects of carbonation. They also collected data from the literature for bars showing pitting corrosion.

Figures 2.6 and 2.7 show the scatter of the experimental data collected for pitting corrosion as well as the experiments conducted by the authors. It can be seen that the data for yield and ultimate stresses is fairly concentrated, whereas it is very scattered for the ultimate strain. Moreover, data pertaining to pitting corrosion show a greater reduction of the mechanical properties of corroded steel.

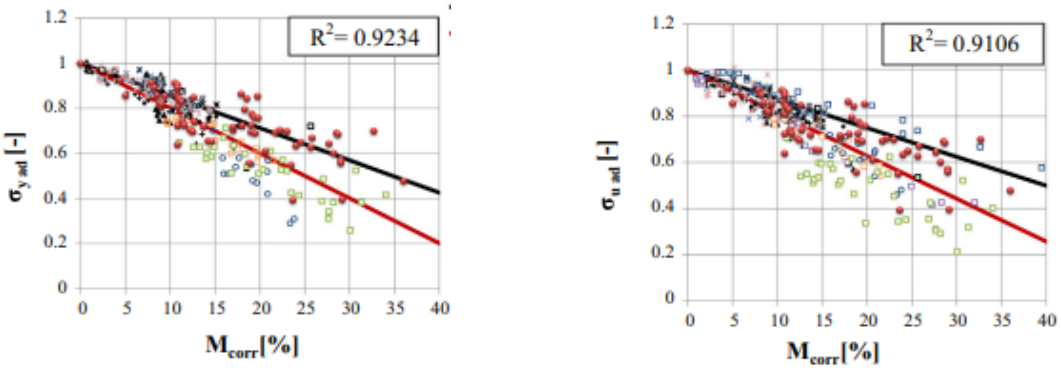

Figure 2.6: Degradation of mechanical properties of corroded bars (yield and ultimate stress)[21]

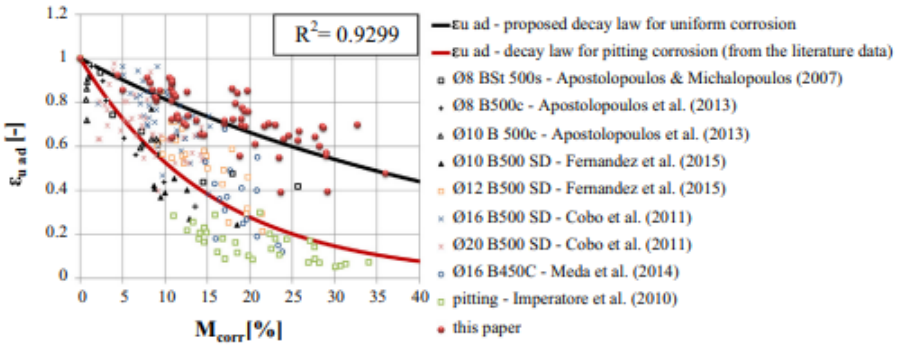

Figure 2.7: Degradation of mechanical properties of corroded bars (ultimate strain)[21]

2.2.3.2 Tests by Ou et al. (2016) [27]

Ou et al. conducted experiment on both naturally corroded steel bars and artificially corroded ones. The naturally corroded bars were taken from a corroded residential building complex located near the sea, and therefore attacked by chlorides.

They started by removing the concrete cover before cutting the bars to obtain samples for tensile tensing. The corrosion level mas measured in terms of average mass loss, as it is easier to assess in practical application than average section loss, and ranges from 6 to 82% for the naturally corroded bars. The bars were then subjected to tensile testing, with a gauge length of approximately eight times the nominal diameter of the uncorroded bar.

Figures 2.8 an 2.9 show that ultimate strain presents more scattered results than yield and ultimate stress as it also depends on the distribution of pits along the bar, whereas the latter properties only depend on the minimum cross-sectional area.

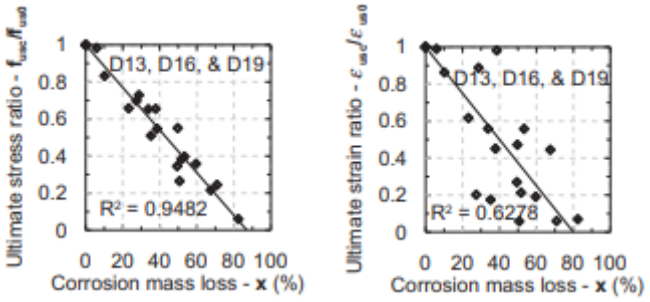

Figure 2.8: Degradation of mechanical properties of corroded bars (ultimate stress and strain) [27]

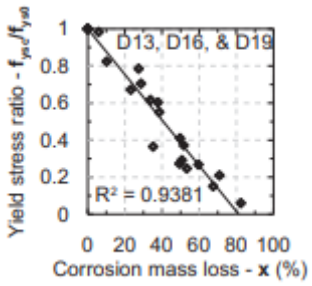

Figure 2.9: Degradation of mechanical properties of corroded bars (yield stress) [27]

2.2.3.3 Tests presented in Bhargava et al. (2007) [6]

To determine their empirical equations for bond strength reduction due to corrosion, Bhargava et al. used data from pullout tests conducted by several authors (Al-Sulaimani et al. (1990) [35], Rodriguez et al. (1994) [32], Cabrera (1996) [8], Almusallam et al. (1996) [2], Amleh and Mirza (1999) [3], Auyeung et al. (2000) [5], Lee et al. (2002) [22], Fang et al. (2004) [19]) with a bar diameter varying between 10 mm and 20 mm. The specimens were subjected to accelerated corrosion by impressed current, and for some of them chlorides ions were incorporated in the cement mix. Corrosion was measured as mass loss except for the specimen cast by Rodriguez et al. where the corrosion was measured in terms of depth of attack corrosion. The corrosion level goes up to 80%. Figure 2.10 shows a summarize of the data of those tests.

Reference	Specimen size (mm × mm × mm)	f'_c (MPa)	f_y (MPa)	D_l (mm)	C (mm)	i_{COR} (μA/cm²)	L (mm)	Corrosion levels	Stirrups
Al-Sulaimani et al. (1990)	150×150×150	30	450	10 Φ	70	2,000	40	0.0–8.75%	Not provided
	150×150×150	30	450	14 Φ	68	2,000	56	0.0–6.50%	Not provided
	150×150×150	30	450	20 Φ	65	2,000	80	0.0–4.35%	Not provided
Rodriguez et al. (1994)	300×300×300	40	590	16 Φ	24	100	210	0.0–0.264 mm	8 Φ at 70 mm c/c
	300×300×300	40	590	16 Φ	24	100	210	0.0–0.351 mm	6 Φ at 100 mm c/c
	300×300×300	40	590	16 Φ	24	100	210	0.0–0.377 mm	Not provided
Cabrera (1996)	150×150×150	Not mentioned	460	12 Φ	69	Constant voltage of 3 V	48	0.0–12.6%	Not provided
Almusallam et al. (1996b)	152×254×279	30	420	12 Φ	63.75	Constant current of 0.4 A	102	0.0–80%	Not provided
Amleh and Mirza (1999)	100 mm diameter ×1,000 mm long	25	432	19.5 Φ	40.25	Constant voltage of 5 V	1,000	0.0–17.5%	Not provided
Auyeung et al. (2000)	177.8×177.8×355.6	28	Not mentioned	19 Φ	79.4	1,944	127	0.0–5.91%	Not provided
Lee et al. (2002)	104×104×104	42.1	315	13 Φ	13–39	Direct current of 1 A	78	0.0–30.0%	Not provided
	104×104×104	33.0	315	13 Φ	13–39	Direct current of 1 A	78	0.0–30.0%	Not provided
	104×104×104	24.7	315	13 Φ	13–39	Direct current of 1 A	78	0.0–30.0%	Not provided
Fang et al. (2004)	140×140×180	52.1	289.6	20 Φ	60	Constant current of 0–2 A	80	0.0–6.77%	Not provided
	140×140×180	52.1	289.6	20 Φ	60	Constant current of 0–2 A	80	0.0–4.74%	6 Φ at 40 mm c/c
	140×140×180	52.1	350.9	20 Φ	60	Constant current of 0–2 A	80	0.0–9.02%	Not provided
	140×140×180	52.1	350.9	20 Φ	60	Constant current of 0–2 A	80	0.0–6.01%	6 Φ at 40 mm c/c

Figure 2.10: Experimental investigation [7]

Figure 2.11 shows the scatter of the results of the experiments. It can be seen that for low levels of corrosion (under 4%), the bond strength is actually higher than for uncorroded bars. On the contrary, for corrosion degrees of more than 15%, the bond strength is severely reduced.

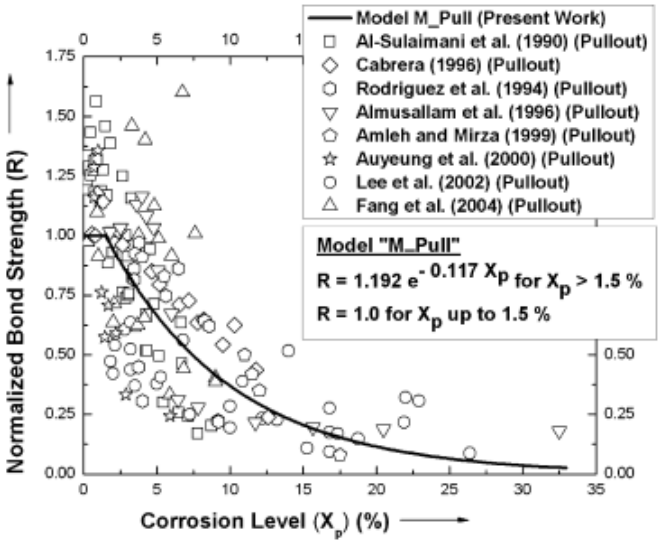

Figure 2.11: Normalized bond strength as a function of corrosion level for experimental data of pullout tests [6]

2.2.3.4 Test by Almusallam et al. (1996)[2]

Almusallam et al. [2] designed an experimental programme to evaluate the bond strength of reinforcement for various degrees of corrosion.

The concrete has a strength of 30 MPa and the bars used have a diameter of 12 mm. The reinforcement was artificially corroded by impressing a direct constant current of 0.4 A on the bars embedded in concrete. The specimens were partially immersed in water, in a way that the reinforcement was completely above the water. The level of corrosion was measured as the weight loss of the reinforcement.

The type of specimen was carefully chosen to evaluate the bond strength as accurately as possible. After comparing different bond test specimens, they decided to perform a cantilever bond test. The specimen had a geometry of 152 × 254 × 279 mm. Figure 2.12 shows the test setup.

Figure 2.13 shows the ultimate bond strength obtained for the various corrosion degrees. A slight increase can be observed for low levels of corrosion. Even before reaching 10% of corrosion, the bond strength drops to a third of its initial value, then decreases slowly to 10% of its value after reaching a corrosion level of about 20%.

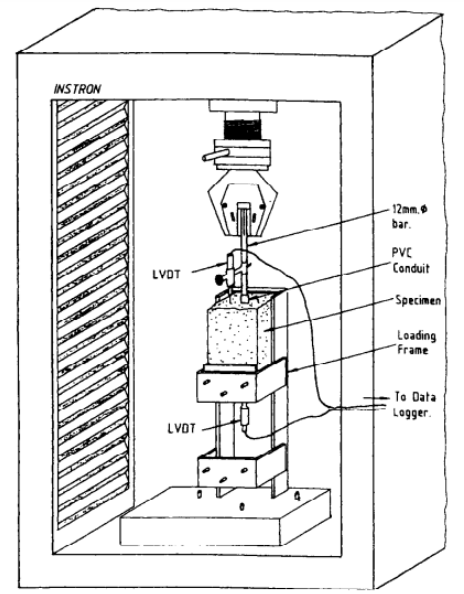

Figure 2.12: Cantilever bond test setup [2]

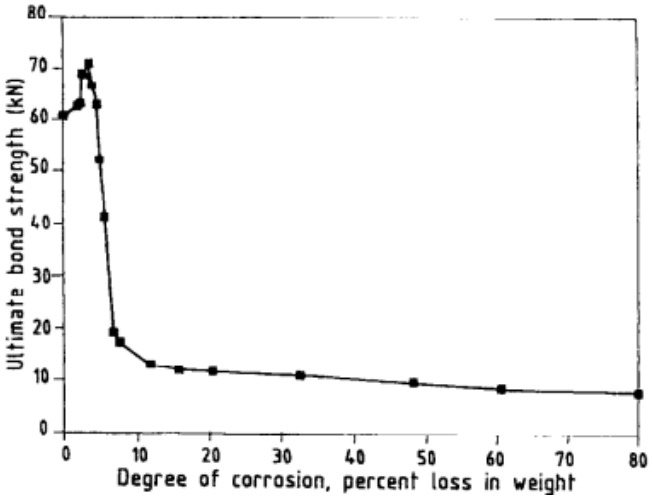

Figure 2.13: Ultimate bond strength as a function of the degree of corrosion [2]

2.3 Tests on corroded dapped-end beams

To validate the model proposed to predict the behavior of corroded dapped-end connections, the predicted values will be compared to experimental data. Two papers presenting the results of tests on corroded dapped-end connections were found. Tests conducted by Rajapakse et al. [31] on uncorroded dapped-end beams will also be used to predict their behavior.

2.3.1 Tests by Di Carlo et al. (2023) [18]

Di Carlo et al. [18] conducted an experimental survey at the Laboratory of the University of Rome "Tor Vergata" to evaluate the behavior of corroded and uncorroded reinforced concrete dapped-ends. A concrete class C30/37 was considered in the design phase of the specimen as well as an Italian B450 steel. The actual properties of the materials are reported in Table 2.2.

Two specimens were designed, one with a low amount of reinforcement (designated as G1-C) and one with high reinforcement amount (designated as G2-C). The beams are 3000 mm long, the nibs have a length of 300 mm and a cross section of 200 mm $\times$ 250 mm, while the internal part of the beam is 500 mm high. The low reinforced specimen is composed of two ϕ10 mm longitudinal rebars in the nib, two ϕ10 mm closed stirrups 50 mm spaced and three ϕ12 mm diagonal rebars. The second specimen is equipped with four ϕ12 mm longitudinal rebars, three ϕ10 mm closed stirrups 50 mm spaced and three ϕ12 mm diagonal rebars. As for reinforcement in compression, four ϕ10 mm bars were used. The concrete cover thickness is 20 mm and the distance between the first stirrup and the inner corner of the nib is 75 mm. Figure 2.14 shows the geometry of the specimens as well as their detailed reinforcement layout and Table 2.1 gives

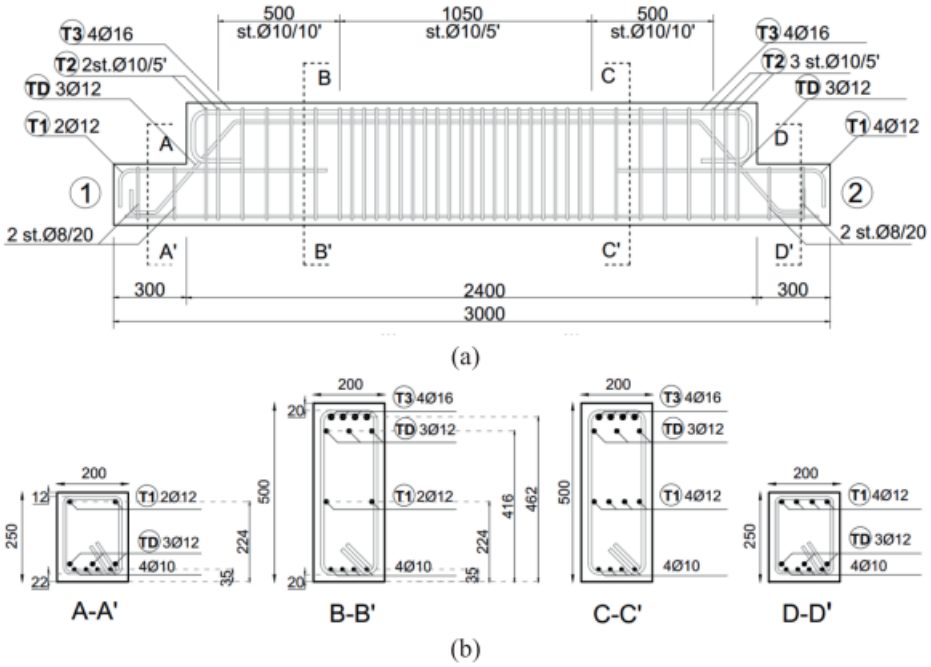

Figure 2.14: Geometry of the specimens and reinforcement layout [18]

the amount of reinforcement and the corrosion degree for each direction of reinforcement.

Reinforcement layout [m]	Steel tie	Reinforcement amount	Corrosion degree
Low	Horizontal	2 ϕ12	21%
	Vertical	2 ϕ10 (2 legs stirrups)	15%
	Diagonal	3 ϕ12	6%
High	Horizontal	4 ϕ12	15%
	Vertical	3 ϕ10 (2 legs stirrups)	18%
	Diagonal	3 ϕ12	8%

Table 2.1: Amount of reinforcement and corrosion degree

Specimens G1-C and G2-C were artificially corroded through an accelerated electrolytic process. As can be seen in Figure 2.15, the beams were placed in a pool filled with a 3% saline solution covering the upper surface of the half-joint. Only the reinforcement close to the nib was connected to the positive pole of a power supply (anode), while the other bars were protected against corrosion by an epoxy coat (Figure 2.16). Two steel bars were placed in the pool near the nibs as cathodes. A current is then applied in order to reach the desired corrosion level of 15%.

The specimens were then tested to evaluate their resistance. After that, the bars were extracted to evaluate the actual degree of corrosion in terms of mass loss. The exact corrosion level of each tie is reported in Table 2.1 and the average corrosion level reached for each specimen was 13% for G1-C and 14% for G2-C. Figure 2.16 shows the corroded bars. The pits depth was also measured and the corrosion morphology as well

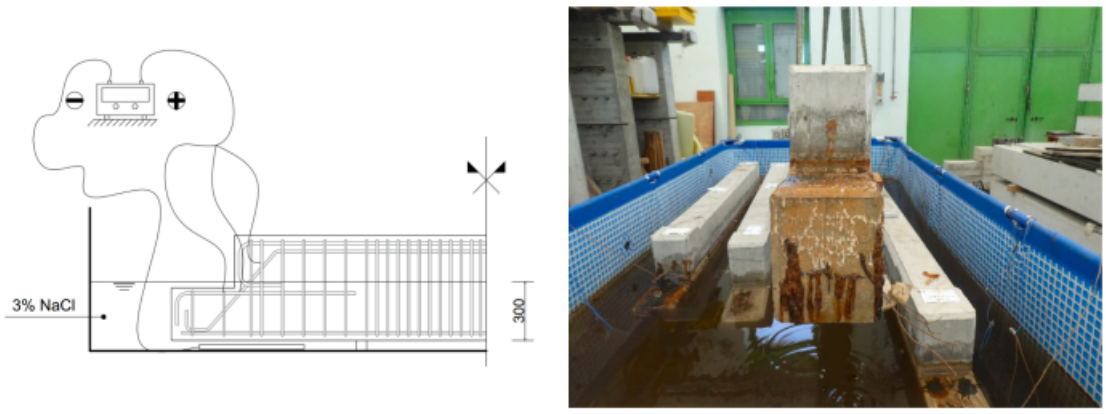

Figure 2.15: Accelerated corrosion process [18]

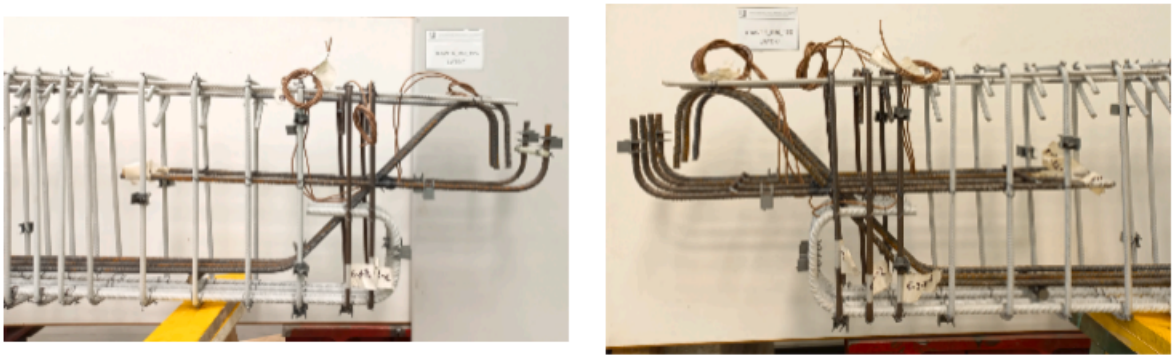

Figure 2.16: Steel cage of the corroded specimens (left : G1-C, right : G2-C) [18]

as the pits location was mapped. Reference specimens were also cast and will be referred to as G1-UC and G2-UC.

2.3.2 Tests by Desnerck et al.[16]

Desnerck et al. [16] also conducted a study on dapped-end beams. Their specimen is 700 mm high and has a reduced height at the nib of 325 mm. It is 3320 mm long and has a depth of 400 mm. The specimen considered in this work is designed with a concrete strength C30/37. The reinforcement in the nib is composed of three U-shaped reinforcing bars with a diameter of 12 mm, and four diagonal ϕ12 mm bars. The shear reinforcement consists of ϕ10 mm two-legged stirrups in the nib, while three-legged stirrups are used in the B-region. The reinforcement in the compression zone consists of five ϕ20 mm bars. Figure 2.17 shows the detailed geometry and reinforcement layout of the specimen.

To study the effect of corrosion, the section of the bars was locally reduced to 50% of the original cross-section in specimen NS-LR by milling down the bars. A reference specimen was also cast and will be referred to as NS-REF.

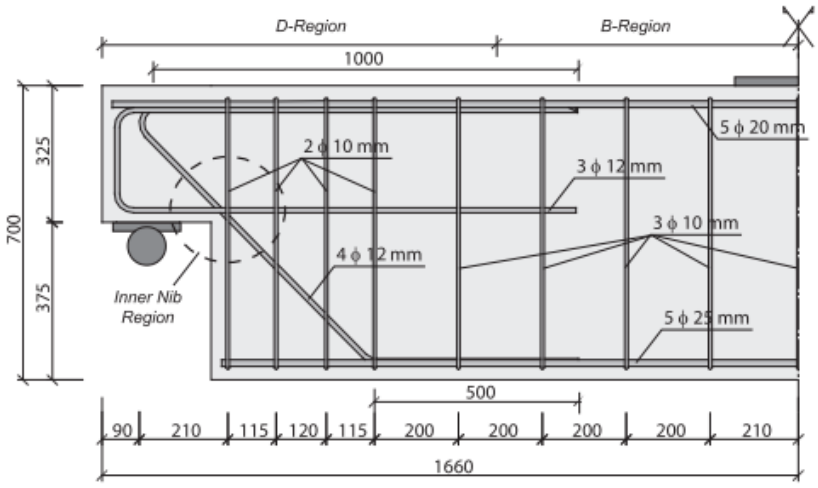

Figure 2.17: Geometry of the specimens and reinforcement layout [17]

2.3.3 Other tests

Tests conducted by Rajapakse et al. [31] will also be used to draw conclusions on corrosion of dapped-end connections although those specimens are not corroded. Figure 2.18 shows the geometry and reinforcement layout of specimens OL3 and OL4.

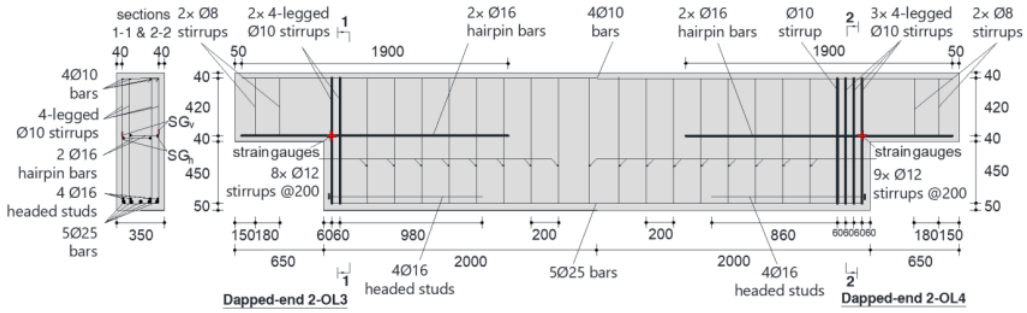

Figure 2.18: Geometry of the specimens and reinforcement layout [31]

Four beams were cast in order to test eight dapped-end configurations. Each half-joint had a different amount of reinforcement, gradually increasing from a specimen to another to observe the different failure modes. The beams had a rectangular cross-section of 1000 mm × 350 mm and a section of 500 mm × 350 mm in the nib of the dapped-end. The beams were 5300 mm long while the dapped-end had a length of 650 mm. From those eight configurations, the medium reinforced dapped-end OL3 and OL4 were selected. The horizontal reinforcement of those specimens consisted of two ϕ16 mm hairpin bars and the vertical reinforcement consisted of two four-legged ϕ10 mm stirrups for specimen OL3 and three four-legged ϕ10 mm stirrups for OL4.

Table 2.2 summarizes the experimental data and gives the experimental peak resistance of each specimen.

Ref.	Beam name	h (mm)	b (mm)	RF_h	f_{yh} (MPa)	A_{sh} (mm^2)	RF_v	f_{yv} (MPa)	A_{sv} (mm^2)	RF_d	f_{yd} (MPa)	A_{sd} (mm^2)	f'_c (MPa)	X (%)	V_{exp} (kN)
[18]	G1-C	250	300	2ϕ12	507.1	226.2	2ϕ10	503.2	157	3ϕ12	507.1	339.3	42	13	166.5
[18]	G1-UC	250	300	2ϕ12	507.1	226.2	2ϕ10	503.2	157	3ϕ12	507.1	339.3	42	0	301.5
[18]	G2-C	250	300	4ϕ12	507.1	452.4	2ϕ10	503.2	157	3ϕ12	507.1	339.3	42	14	247.1
[18]	G2-UC	250	300	4ϕ12	507.1	452.4	2ϕ10	503.2	157	3ϕ12	507.1	339.3	42	0	331.8
[17]	NS-LR	325	260	3ϕ12	529	339.3	2ϕ10	539	157	4ϕ12	529	452.4	33.8	50	261.9
[17]	NS-REF	325	260	3ϕ12	529	339.3	2ϕ10	539	157	4ϕ12	529	452.4	33.8	0	402.3
[31]	OL3	500	350	2ϕ16	599.2	804	2ϕ10	509.1	157	/	/	/	56	0	472
[31]	OL4	500	350	2ϕ16	599.2	804	3ϕ10	509.1	314	/	/	/	56	0	555
[31]	OL1	500	350	2ϕ12	537	452	2ϕ8	521	301	/	/	/	56.8	0	245
[31]	OL8	500	350	2ϕ25	540	1964	6ϕ12	537	2712	/	/	/	52	0	995

Table 2.2: Experimental data for corroded dapped-ends

Chapter 3

Extended model for behavior of corroded dapped-end connections

To extend the model developed by Rajapakse et al. to include the effects of corrosion on the resistance of dapped-end connections, two modifications will be made.

First, the stress-strain relationship of the steel reinforcement will be modified to account for the degradation of mechanical properties due to corrosion. Three models are discussed in section 3.1 and will later be compared.

Second, the extended model will also account for the reduction of bond strength between the concrete and the steel reinforcement due to corrosion. Two empirical models are proposed in section 3.2.

Once one model is chosen to represent each of these effects, they will be implemented in the kinematic-based model to predict the resistance and complete behavior of corroded dapped-end beams.

3.1 Stress-strain relationship for corroded steel reinforcement

As explained in section 2.2, corrosion reduces the cross-section of steel reinforcement. This effect can be modelled in two ways : either by calculating the reduced area of reinforcement, or by computing the stress-strain relationship of the corroded bars [14]. Campione et al. [11] proposed a model for the first option. However, it requires to know the depth of the pits, which is an information that is not always available in practice. On the other hand, several other authors conducted experimental studies to determine stress-strain relationships of the corroded reinforcement, depending only on the corrosion degree of the bar. Empirical models correlating residual strength and ductility with section loss are more practical since there is usually no information on the topography of the corrosion of the bars [10].

The stress-strain relationship of steel reinforcement is modelled by a bi-linear curve. The first branch of this curve is the elastic response of steel while the second part is the yield plateau with strain-hardening effect. Several authors proposed degradation equations to assess the residual mechanical properties of corroded steel bars. A selection of those equations is presented below. They usually take the form of a linear regression :

$$\beta = 1 - \alpha X \tag{3.1}$$

where β is the property considered, such as the yield strength f_y, the ultimate strength f_u or the ultimate strain ϵ_u. X is the corrosion level, usually expressed as a mass loss or section loss and α is the reduction coefficient. The latter is determined empirically. The proposed values for those coefficients are based on different corrosion methods, corrosion types or different tests. A value of α superior to 0.01 for f_y and f_u is usually a sign of pitting corrosion, while a lower value corresponds to a more uniform corrosion.

3.1.1 Coefficients proposed by Imperatore et al. (2017) [21]

Imperatore et al. proposed values for the reduction coefficients α based on the tests presented in section 2.2.3.1. A statistical approach was used to determine the coefficients. A linear regression was found to be the best fit for the yield and ultimate strengths while an exponential regression was used for the ultimate strain.

Imperatore et al. propose coefficients for both uniform and pitting corrosion. In this work, pitting corrosion is more relevant seeing as the half-joints are attacked by chlorides, which usually produce more localized corrosion. The proposed degradation equations are the following:

$$\begin{cases} f_{y,corr} = (1 - 0.019961X) f_y \\ f_{u,corr} = (1 - 0.018642X) f_u \\ \epsilon_{u,corr} = e^{-0.0546993X} \epsilon_u \end{cases} \tag{3.2}$$

Figure 3.1 shows the stress-strain relationship obtained with the degradation equations 3.2 for different degrees of corrosion. It can be seen that the strength decreases drastically for 40% of corrosion and even more for 50% of corrosion. The stress-strain relationship for 50% of corrosion doesn't seem realistic as the bar would lose all its strength. Therefore, although the model is valid for corrosion levels up to 53%, it may not be the most appropriate model for such corrosion degrees. The ductility of the bars is also greatly reduced as the corrosion level increases.

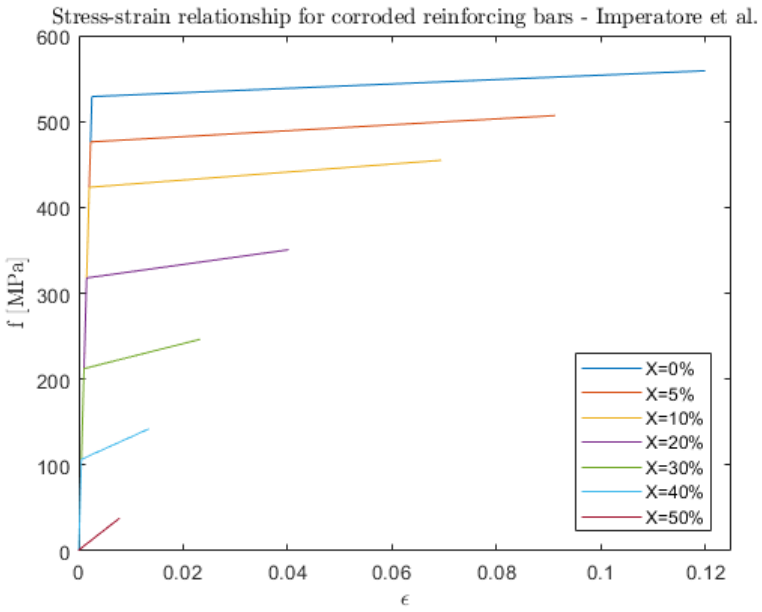

Figure 3.1: Stress-strain relationship proposed by Imperatore et al.

The reduction of yield strength will have an impact on the strength of the dapped-end connection. The shortening of the yield plateau and thus the reduction of ductility is also very significant for the plastic analysis [10].

3.1.2 Coefficients proposed by Morinaga (2004) [25]

In Cairns et al. 2005 [10], the authors present their own reduction coefficients as well as coefficients proposed by other authors. As the range of validity for their coefficients is very small (between 0% and 3% of corrosion) and therefore not very interesting in this study, they will not be presented. However, among the coefficients proposed by other authors, the ones proposed by Morinaga stood out as they were calibrated based on bars corroded in service by chlorides, which corresponds to the case studied in this work.

Morinaga proposed the following equations, and they are valid for a degree of corrosion varying between 0 and 25% :

$$\begin{cases} f_{y,corr} = (1 - 0.017X) f_y \\ f_{u,corr} = (1 - 0.018X) f_u \\ \epsilon_{u,corr} = (1 - 0.06X) \epsilon_u \end{cases} \tag{3.3}$$

Figure 3.2 shows the stress-strain relationship of corroded bars obtained with Morinaga's equations. As for the model proposed by Imperatore et al., a reduction of the yield and ultimate strength as well as a shortening of the yield plateau, which results in a significant reduction of ductility, are observed.

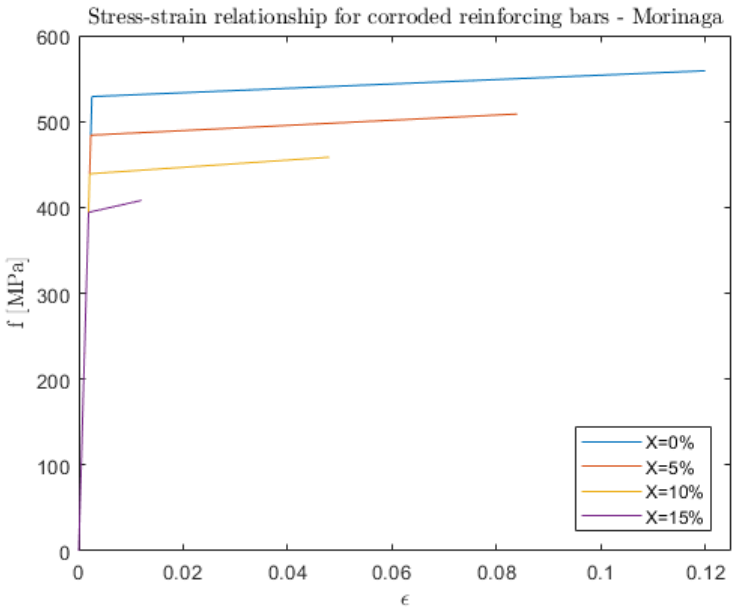

Figure 3.2: Stress-strain relationship proposed by Morinaga

3.1.3 Coefficients proposed by Ou et al. (2016) [27]

Based on the experiment conducted by the authors described in section 2.2.3.2, the following equations were derived for naturally corroded bars :

$$\begin{cases} f_{y,corr} = (1 - 0.0123X) f_y \\ f_{u,corr} = (1 - 0.0115X) f_u \\ \epsilon_{u,corr} = (1 - 0.0125X) \epsilon_u \end{cases} \tag{3.4}$$

Those equations are valid for corrosion levels up to 80%. Figure 3.3 shows the idealized stress-strain curve for various corrosion degrees. The reduction of both yield strength and ductility is less pronounced than what is observed for Imperatore et al. and Morinaga's models.

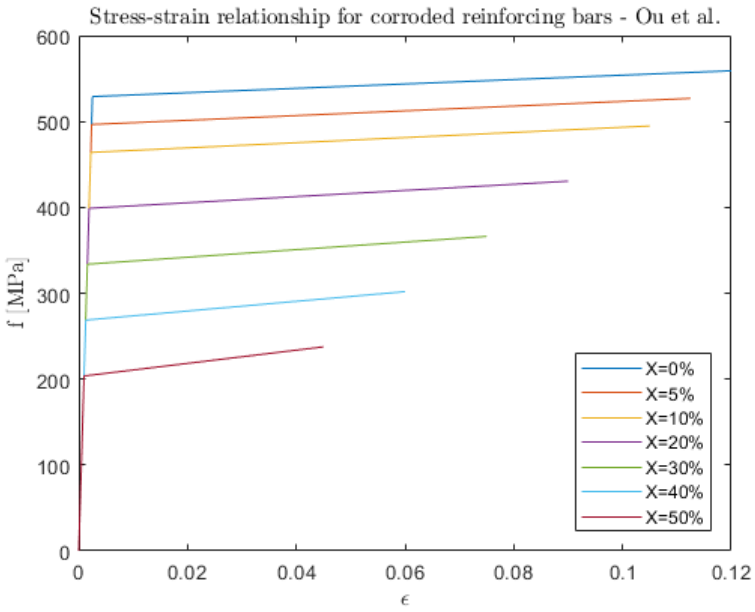

Figure 3.3: Stress-strain relationship proposed by Ou et al. [27]

3.2 Model for reduced bond strength due to corrosion

Corrosion has also an impact on the bond strength between concrete and the reinforcement as explained in section 2.2. Several models exist to assess this reduction of bond such as finite element models, analytical models, or empirical models.

Regarding finite element models, Lundgren et al. (2002) [24] proposed a 3D FE model with frictional bond model to account for the effect of the ribs of the bar and a corrosion model that can be seen as a separate layer. For analytical models, Cairns and Abdullah (1996) [9] proposed an adaptation of the analytical model proposed for splitting bond failure by Coronelli (2002) [13] to account for corrosion of the reinforcement. However, this model depends on a lot of parameters, some of them being difficult to assess. Bhargava et al. (2007) [6] propose estimation of parameters such as corrosion pressure, confining action of cracked concrete and shear stirrups after incorporating the effect of corrosion products and adhesion and friction between steel and cracked concrete.

In this work, empirical models will be presented since they only depend on the corrosion level, which is more practical, as the other models depend on many variables that wouldn't be easy to quantify.

The empirical models developed in the next sections seek to derive the normalized bond strength ratio R to apply to the maximum bond strength. The reduced bond strength due to corrosion can then be calculated as :

$$\tau_b = Rkf_{ct} \tag{3.5}$$

where f_{ct} is the tensile strength of concrete, k is the bond reduction factor calculated from Eq. 2.9 and R is the normalized bond strength ratio.

3.2.1 Empirical model proposed by Bhargava et al. (2007)[6]

Based on the experimental data presented in section 2.11, the following empirical formulae are proposed by Bhargava et al. [6] to evaluate the degradation of bond between the concrete and the reinforcement due to corrosion :

$$\begin{cases} R = 1.0 & \text{for } X \leq 1.5 \\ R = 1.192e^{-0.117X} & \text{for } X > 1.5 \end{cases} \tag{3.6}$$

Figure 3.4 illustrates the obtained normalized reduction of bond. In this model, there is a short plateau up until 1.5% corrosion degree, then the bond strength decreases rapidly and is almost equal to zero when a corrosion degree of 30% is reached. Figure 2.11 shows the same curve with the experimental data. It can be seen that the data is quite scattered for low corrosion levels and that the plateau might underestimate the bond strength in those early stages.

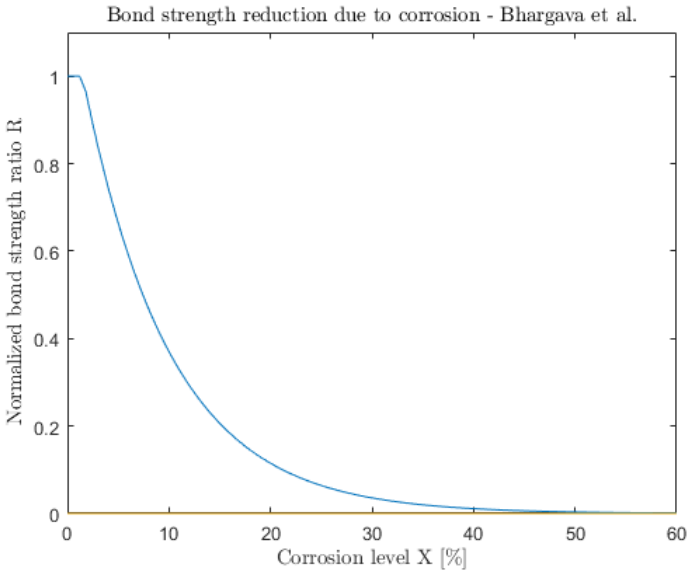

Figure 3.4: Normalized bond strength as a function of corrosion level

3.2.2 Empirical model proposed by Li et al. (2014) [23]

The empirical model proposed by Li et al. is solely based on the experiments conducted by Almusallam et al. [2] described in section 2.2.3.4. The following formulae are proposed :

$$\begin{cases} R = 0.9959e^{0.0041X} + 0.0069e^{0.7858X} & \text{for } X \leq 4 \\ R = 9.662e^{-0.5552X} + 0.1887e^{-0.0069X} & \text{for } X > 4 \end{cases} \tag{3.7}$$

Figure 3.5 shows both the proposed empirical model and the data used. First of all, compared to the model proposed above by Bhargava et al., Li et al.'s model increases the bond until a degree of corrosion of 4%. After that the bond decreases until it reaches a value of approximately 10% of the initial bond.

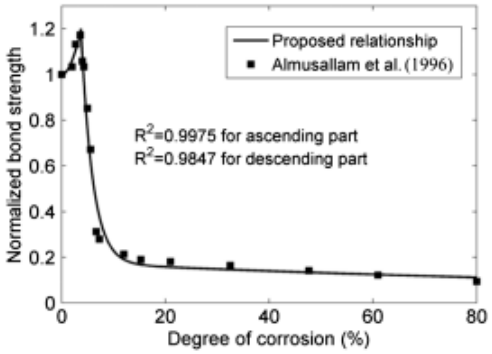

Figure 3.5: Deterioration of maximum bond strength as a function of corrosion [23]

Chapter 4

Comparisons with tests

In the first part of this chapter, the models proposed in the previous chapter are compared in order to select only one model for each effect. In the second part, the complete extended model is applied to the corroded specimens presented in section 2.3 to compare the experimental results to the results predicted by the extended kinematic-based model.

4.1 Comparison of stress-strain relationships for corroded reinforcement

Figures 4.1 and 4.2 show the maximum strength of the specimens considering only the modification of the stress-strain relationship as an effect of corrosion. As can be seen for specimens G1-C and G2-C in Figure 4.1, the different models give similar results in that range of corrosion degree.

For G1-C, all the proposed models overestimate the strength of the dapped-end, with the model proposed by Imperatore et al. being the closest to the experimental results. As for G2-C, the model proposed by Imperatore et al. is again the closest and is also the only one to underestimate the results. The other two models overestimate the value of the resistance.

Finally, for specimen NS-LR, the model proposed by Ou et al. gives the closest results as can be seen in Figure 4.2. All models strongly underestimate the strength of this specimen. The difference between the models is more marked than for the previous specimens. Obviously, the model proposed by Morinaga is not suitable for this specimen, as the degree of corrosion is outside the model's range of validity. The other two models give rather different results as the coefficients proposed by Imperatore et al. are more penalizing than those proposed by Ou et al.

The model chosen for the rest of this work is the one proposed by Ou et al. as it is the best compromise for all specimens.

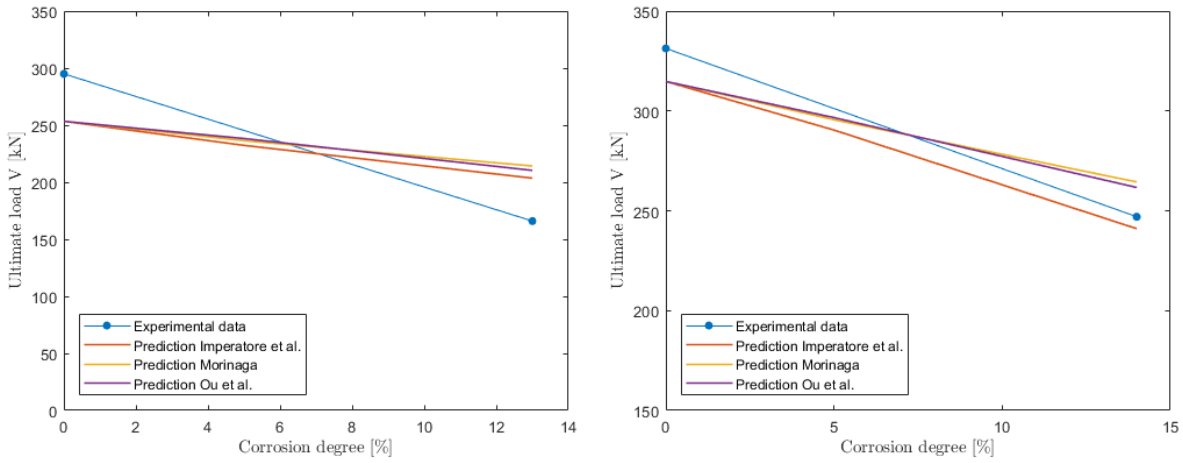

Figure 4.1: Comparison between the models for specimens G1-C (left) and G2-C (right)

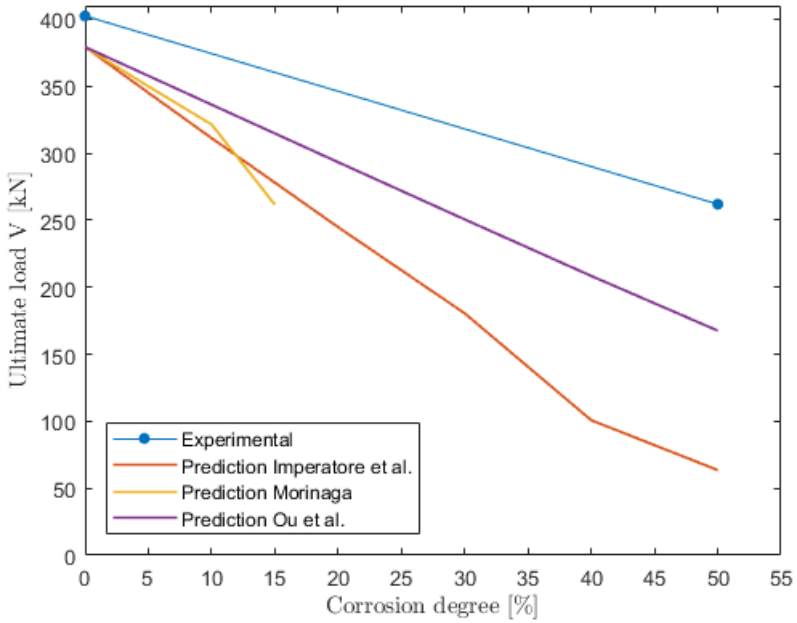

Figure 4.2: Comparison between the models for specimen NS-LR

4.2 Comparison of models for bond strength reduction

Although the two presented models for bond reduction are quite different, those differences are barely noticeable once the models are implemented in the kinematic-based model. Figure 4.3 and 4.4 show the peak resistance of the specimens when only modifying the bond strength between the concrete and the reinforcement.

After 20% of corrosion, Li et al. model suggests that the remaining bond strength is only equal to 10% of the original bond strength, while Bhargava et al. model assumes

that there is no more bond strength after 30% corrosion. Therefore, the estimated value of the ultimate load for specimen NS-LR (Figure 4.4) after 30% corrosion is the ultimate load if there is no bond between the concrete and the reinforcement, whereas there is still 10% of bond in the model proposed by Li et al.

It can also be concluded that the reduction of bond strength alone cannot explain the reduction of the ultimate strength of the dapped-end connections as there is a big gap between the predicted resistance and the experimental results for every specimen.

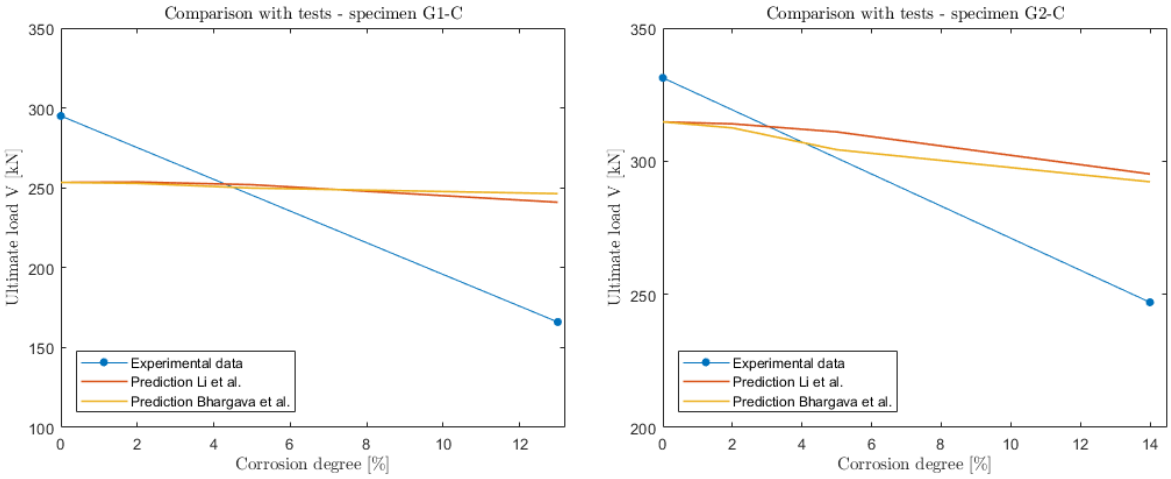

Figure 4.3: Comparison between the bond strength models for specimens G1-C (left) and G2-C (right)

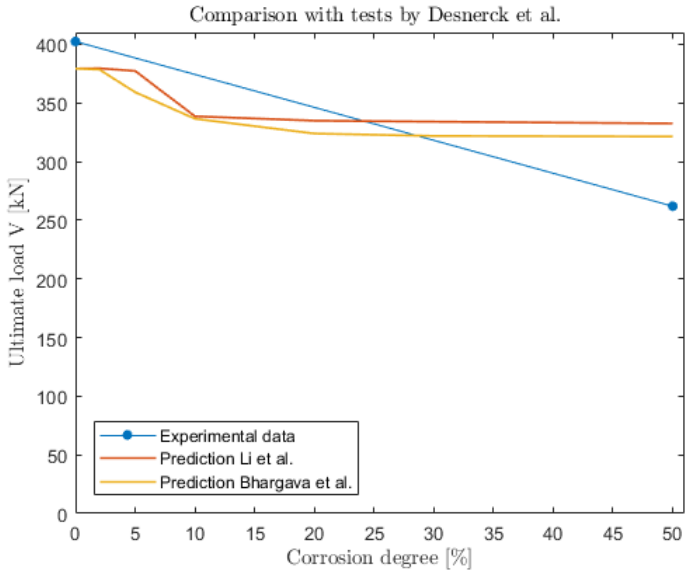

Figure 4.4: Comparison between the bond strength models for specimen NS-LR

Finally, the model chosen to continue this study is the one proposed by Li et al. since there is no big difference in the results and that it depicts more accurately the behavior

of bond for corroded rebars.

4.3 Complete extended model for corrosion effects

Now that a model for the stress-strain relationship of corroded reinforcement and a model for the reduction of bond strength due to corrosion have been chosen, it is possible to compute the complete behavior of corroded dapped-end connections. To validate this modelling, the tests by Di Carlo et al. [18] and Desnerck et al. [17] described previously are used.

Figure 4.5 shows the resistance of specimen G1-C for various degrees of corrosion. The model overestimates the resistance of the corroded specimen by 44 kN.

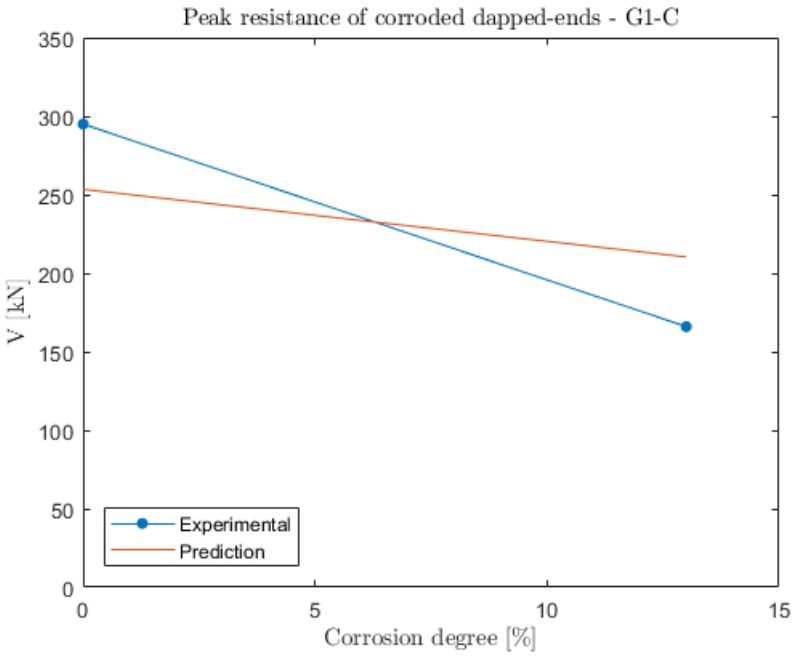

Figure 4.5: Evaluation of the peak resistance of corroded dapped-ends - specimen G1-C

Figure 4.6 shows the results obtained for specimen G2-C. Again, the predicted resistance is higher than what is observed experimentally. However, the gap between the predicted and experimental results is narrowing compared to the results for specimen G1-C. The predicted results are quite satisfying for this specimen.

As for specimen NS-LR, Figure 4.7 shows that its resistance is strongly underestimated by the extended model. As a reminder, this specimen has not undergone any corrosion process. The cross-sections of the bars have been reduced to mimic the effect of corrosion. This could explain the difference between the experimental results and the strength predicted by the model as it does not accurately represent the effects corrosion

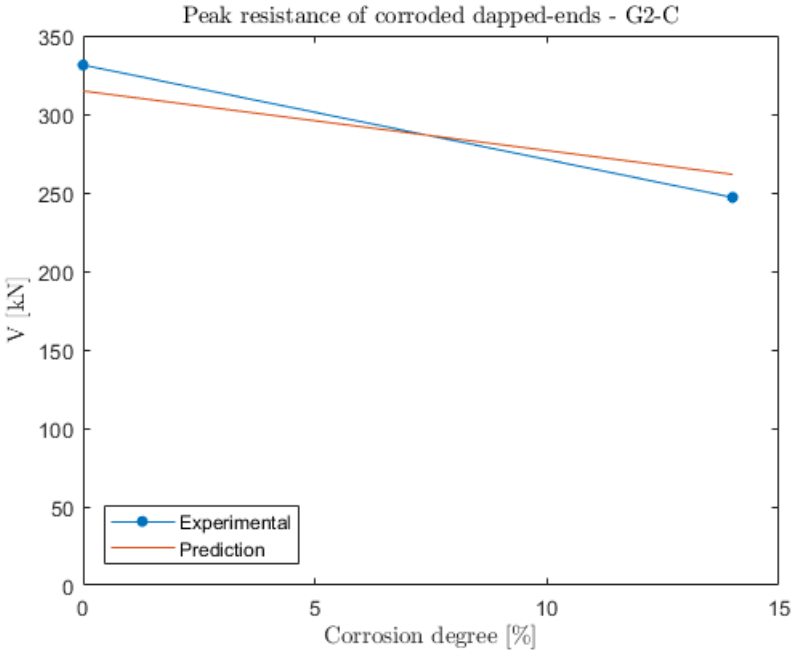

Figure 4.6: Evaluation of the peak resistance of corroded dapped-ends - specimen G2-C

can have on a reinforcing bar.

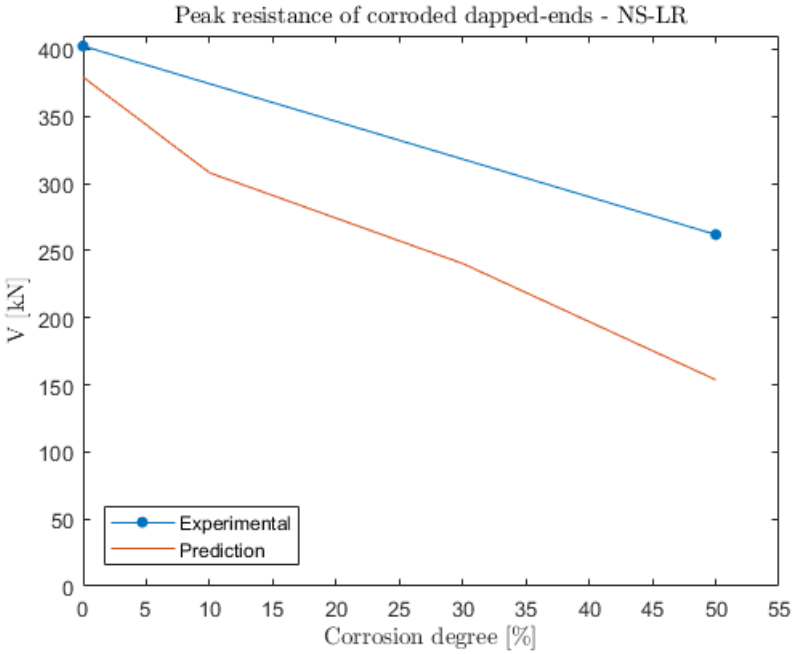

Figure 4.7: Evaluation of the peak resistance of corroded dapped-ends - specimen NS-LR

Another reason that might explain those results is that both the reduction of the steel properties and the reduction of bond are applied on every bar in the model, and not just the corroded ones, and on their total length instead of locally in the nib region.

Other reasons why the predicted resistance and the experimental data differ might be that the specimens used to calibrate the degradation equations and bond strength reduction are subjected to accelerated corrosion, which leads to more a uniform section loss than service conditions [10]. It could also be because the corroded dapped-end connections from the database are not corroded while loaded [23], which does not accurately represent the real situation of such structures.

Chapter 5

Parametric study

In this chapter, several parameters will be studied to determine their influence on the behavior of the dapped-end connections. The parameters studied are the corrosion and its effect on the opening of the cracks, the impact of mean corrosion or exact corrosion, and the behavior of more reinforced corroded dapped-ends compared to lighter reinforced ones.

5.1 Effect of corrosion on the opening of cracks

Figures 5.1 to 5.3 show the support shear vs. crack width response. It is computed for all the dapped-end connections presented and for different corrosion degrees.

As can be seen on those Figures, the corrosion has two main effects : it decreases the resistance of the dapped-end and it increases the width of the cracks.

The first effect is logical as the yield strength of the bars is reduced. The second one suggest a more ductile behavior of the dapped-ends, contrary to previous observations made on the impact of corrosion on reinforcing bars. This could be explained by the fact that reducing bar strength has a similar effect to using smaller diameter bars [14] and, as demonstrated in Rajapakse et al. [31], has the effect of increasing crack width. So as the amount of reinforcement is increased, the failure mode shifts from ductile to brittle, suggesting that less reinforced dapped-end exhibit a more ductile behavior. Therefore, as the reinforcement is corroded, the dapped-end acts as if less reinforced and demonstrates a more ductile behavior.

Figure 5.4 shows the behavior of specimen OL1 and OL8 from the investigation conducted by Rajapakse et al., which were respectively the specimen with the lowest amount of reinforcement and the highest amount of reinforcement. From this figure, it can be observed that as the dapped-end connection becomes more corroded, its behavior becomes similar to that of a lighter reinforced half-joint. Moreover, the crack opening becomes wider for lighter reinforced specimen as their reinforcement yields. The reinforcement of specimen more heavily reinforced doesn't yield and the dapped-end fails from crushing of the concrete.

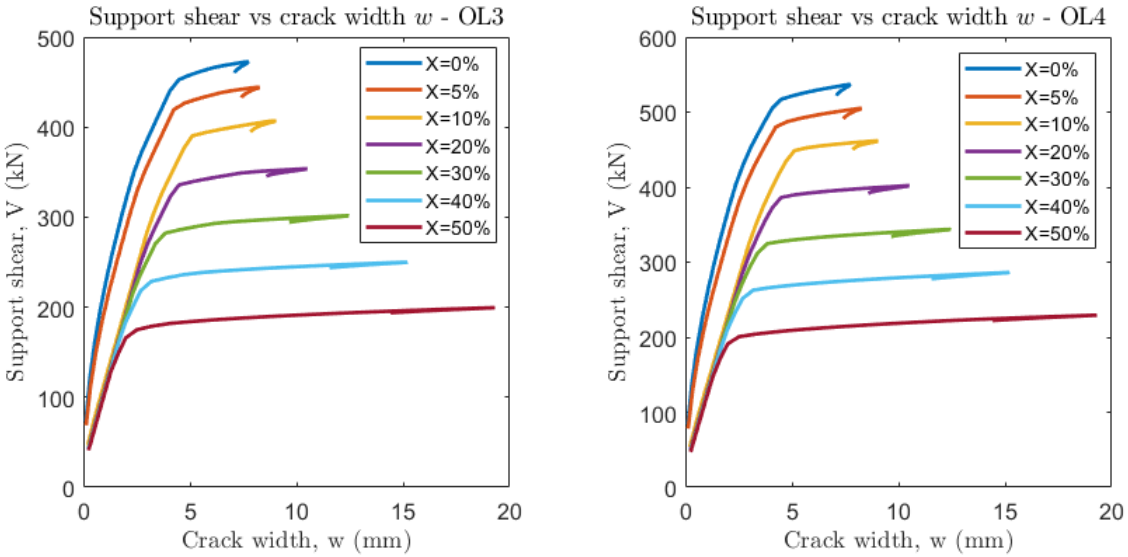

Figure 5.1: Complete behavior of specimens OL3 (left) OL4 (right)

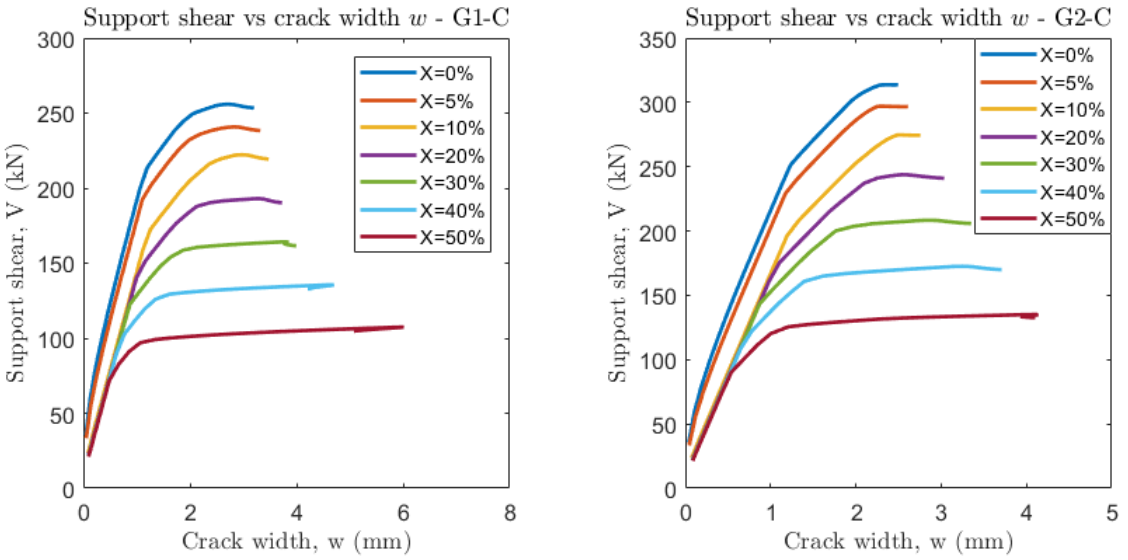

Figure 5.2: Complete behavior of specimens G1-C (left) and G2-C (right)

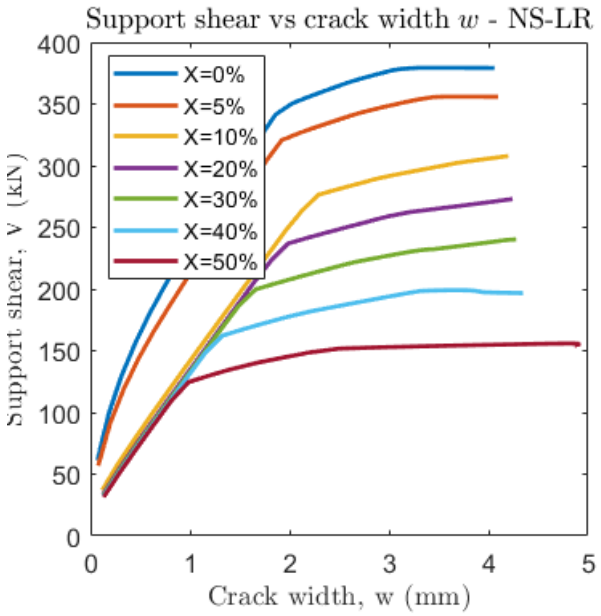

Figure 5.3: Complete behavior of specimen NS-LR

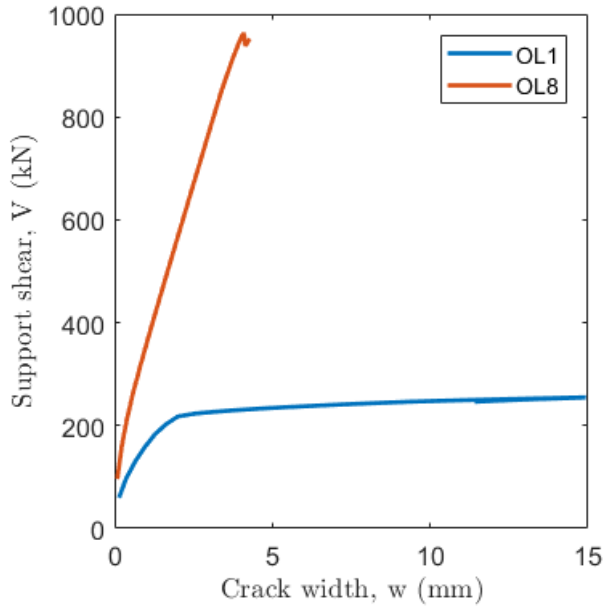

Figure 5.4: Complete behavior of uncorroded specimens OL1 and OL8

The crack opening of specimens G1-C, G2-C and NS-LR is however lower than what is predicted for specimens OL3 and OL4. The crack opening of the former does not exceed 5 mm, whereas the crack opening reaches 20 mm for the latter.

5.2 Exact corrosion degree vs. mean corrosion degree

For specimens G1-C and G2-C, the corrosion degree was measured for the horizontal, diagonal and vertical reinforcement before calculating the average corrosion degree for each specimen. Figures 5.6 and 5.7 give the ultimate load of each specimen for both mean corrosion degree and exact corrosion degree in order to compare the two and determine if average corrosion is a good substitute.

Another way of expressing the amount of corrosion is also studied. So far, the same corrosion degree was applied on all bars. However, the bars probably won't exhibit the same degree of corrosion in practice. It is assumed that the bars with the smallest diameter will exhibit the highest level of corrosion. The corrosion level of the bigger bars is then evaluated by assuming that the diameter of the bars is reduced by the same amount for all bars. Figure 5.5 illustrates this assumption.

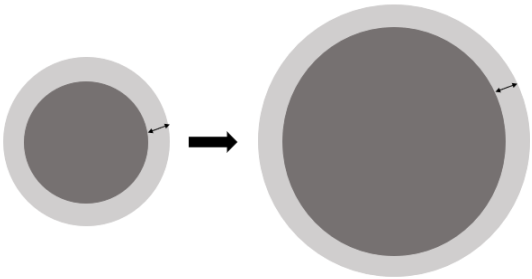

Figure 5.5: Same reduction of diameter for all reinforcing bars

For specimen G1-C, the distribution of corrosion found with this method to obtain a mean degree of corrosion of 13% is a degree of corrosion of 15% for the stirrups and of 12.58% for the other bars. For specimen G2-C, the mean corrosion degree is 14% and the new distribution is 16% for the stirrups and 13.43% for the other bars. Finally, for specimen NS-LR, the ultimate load is evaluated for corrosion levels of 10%, 30% and 50%. The distribution for 10% corrosion is 11.5% for the stirrups and 9.63% for the other bars, for 30% it is 34% and 28.82% and for 50% corrosion it is 55.5% for the stirrups and 47.79% for the horizontal and diagonal reinforcement.

The real corrosion degree gives a higher ultimate load in both cases and is close to the ultimate load given for mean corrosion degree. The results obtained by not distributing uniformly the corrosion level between the bars gives the same results as those obtained with the mean corrosion degree, suggesting that the assumption made above is valid.

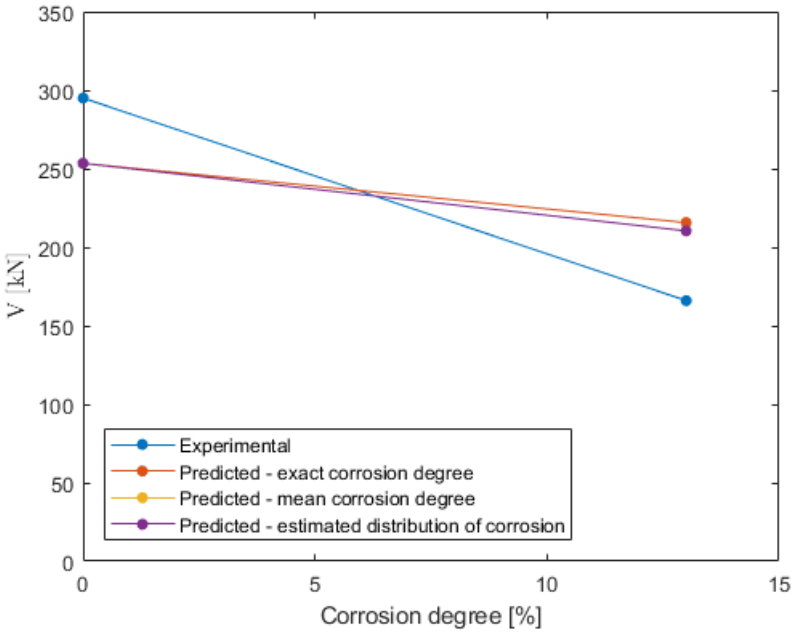

Figure 5.6: Comparison between exact and mean degree of corrosion - G1-C

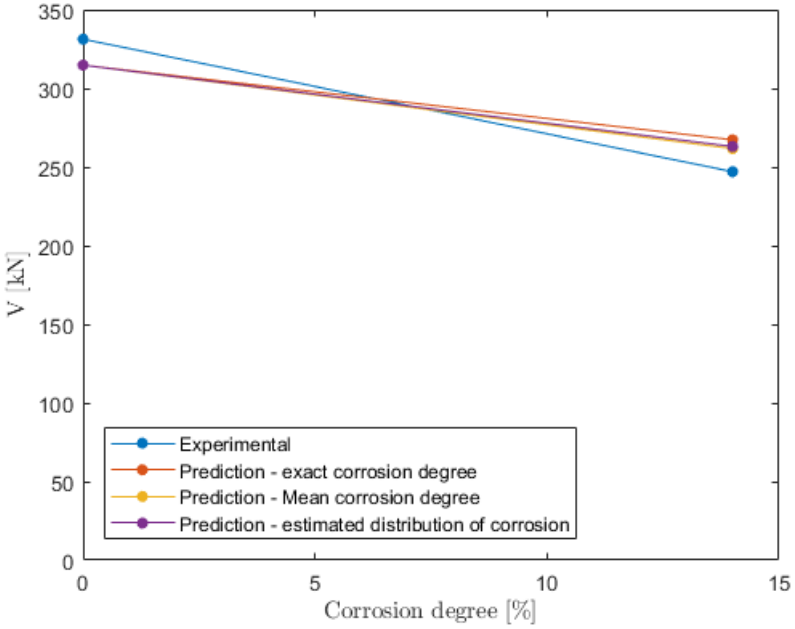

Figure 5.7: Comparison between exact and mean degree of corrosion - G2-C

From Figures 5.6 and 5.7, it can be concluded that mean corrosion degree is a good substitute for the exact corrosion degree for those specimens as it gives results close to the experimental value and safer than the exact degree of corrosion.

Figure 5.8 shows that the new distribution of corrosion is even more severe than the prediction with mean corrosion for specimen NS-LR.

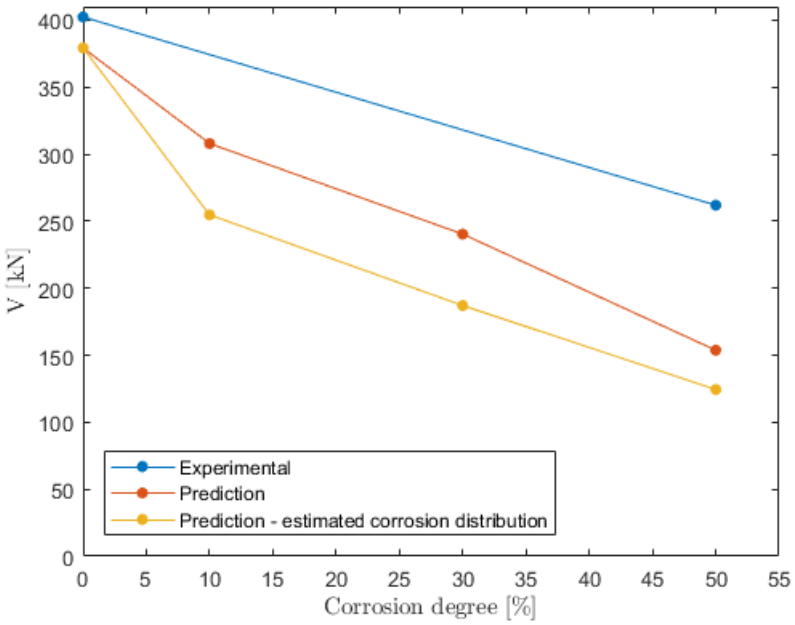

Figure 5.8: Comparison between exact and mean degree of corrosion - NS-LR

5.3 Influence of reinforcement amount

Finally, the effect of corrosion can be studied depending on the reinforcement amount. Specimens OL3 and OL4 [31] and G1-C and G2-C [18] defer only on the amount of reinforcement used. Each pair of specimen has the same geometry and only the number of bars used varies.

Figure 5.9 shows a steeper decline of the resistance for the more reinforced specimen (OL4). To try to explain this phenomenon, the resistance was plotted depending on the amount of reinforcement. In Rajapakse et al. [31] experimental program, four beams were cast, gradually increasing the reinforcement and with a dapped-end presenting a heavier vertical reinforcement amount for each beam. The solid lines of Figure 5.10 represent the resistance of those 8 uncorroded dapped-ends depending on their reinforcement amount. The dots represent the predicted resistance of specimens OL3 and OL4 when modelling corrosion. It can be seen that the corrosion of OL3 follows the blue curve, suggesting that even though the reduction of section isn't modelled explicitly, the model accurately represents the loss of cross-sectional area of the bars for specimen OL3. However, specimen OL4 doesn't follow the orange curve and instead gets closer to the behavior of OL3.

To understand what could cause this discrepancy, two options were explored. The first one is to compute the peak resistance of the corroded specimens without accounting for the reduction of bond strength due to corrosion. The second one is to calculate the percentage by which the yield strength of the steel is reduced and to reduce the area of reinforcement by the same percentage instead of reducing it by the degree of corrosion as done for Figure 5.10.

Figure 5.11 shows on the left the results for the first option. It can be seen that the curve corresponding to specimen OL4 gets closer to the orange curve, meaning that the reduction of bond strength could indeed explain the difference in results. However, the curve for OL3 doesn't fit as well as in Figure 5.10. It can also be noted that the last points from OL4's curve get further from the orange curve. Indeed, the vertical reinforcement for this level of corrosion has ruptured and therefore the resistance drops.

Figure 5.11 shows on the right the results for the second option. Again, the curve corresponding to OL4 gets closer to the orange curve and the curve corresponding to OL3 gets farther from the blue one. However this option seems to be a better compromise than the previous one.

Finally, both options are combined on Figure 5.12. Here, the curve for specimen OL4 fits almost perfectly on the orange curve, whereas the one for OL3 doesn't fit anymore on the blue one.

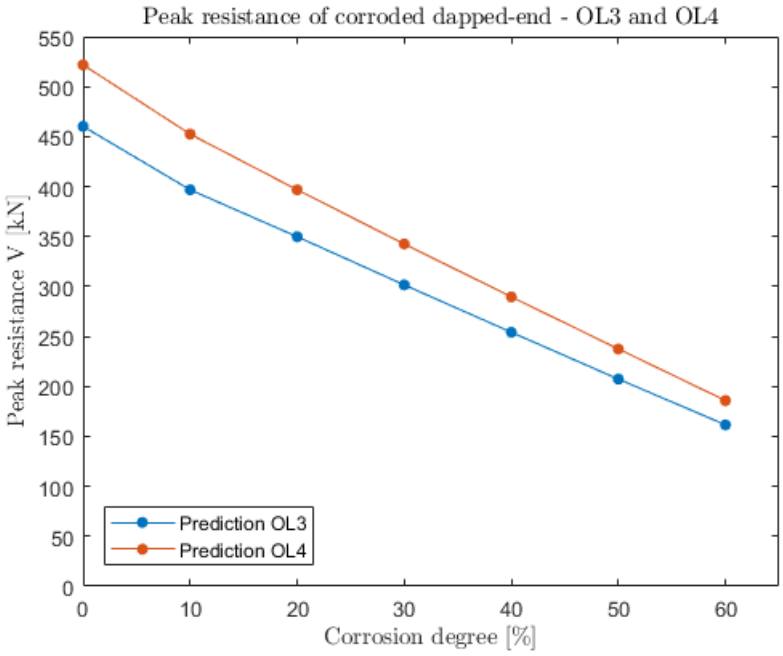

Figure 5.9: Effect of reinforcement amount - Rajapkse et al. specimen [31]

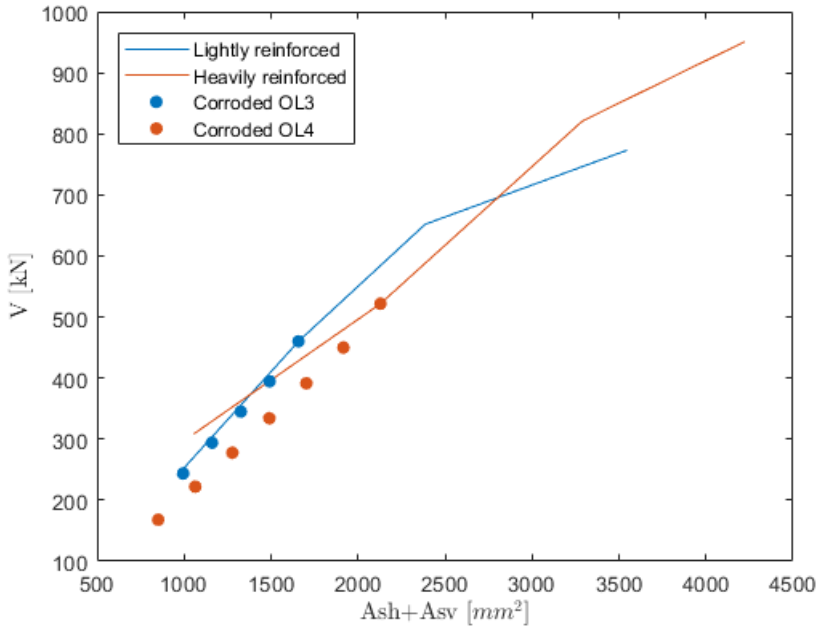

Figure 5.10: Resistance of the dapped-end as a function of reinforcement amount

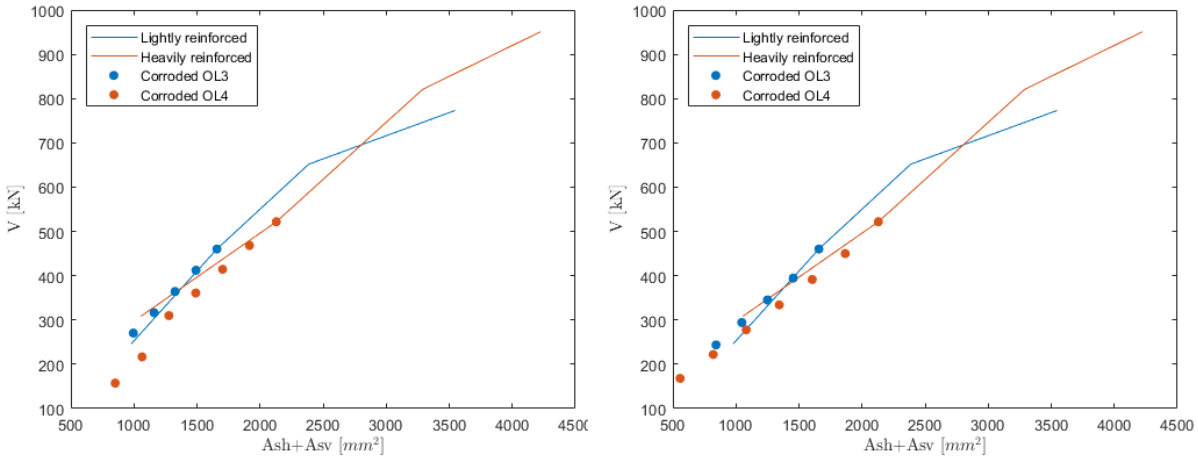

Figure 5.11: Resistance as a function of the amount of reinforcement evaluated without bond reduction (left) and with the same reduction of section as the reduction of yield strength (right)

Figure 5.13 shows the same behavior as in Figure 5.10 for the specimens studied by Di Carlo et al. : the resistance of specimen G2-C decreases more rapidly than the resistance of G1-C, even though it is less visible here.

Figure 5.14 shows the decrease of resistance between specimens G2-C and G1-C (solid line) and the decrease of resistance when specimen G2-C is corroded (dots). In this case, G2-C doesn't follow the same trend as for the reduction of reinforcement amount. Its resistance is much smaller than for the uncorroded specimen with less reinforcement.

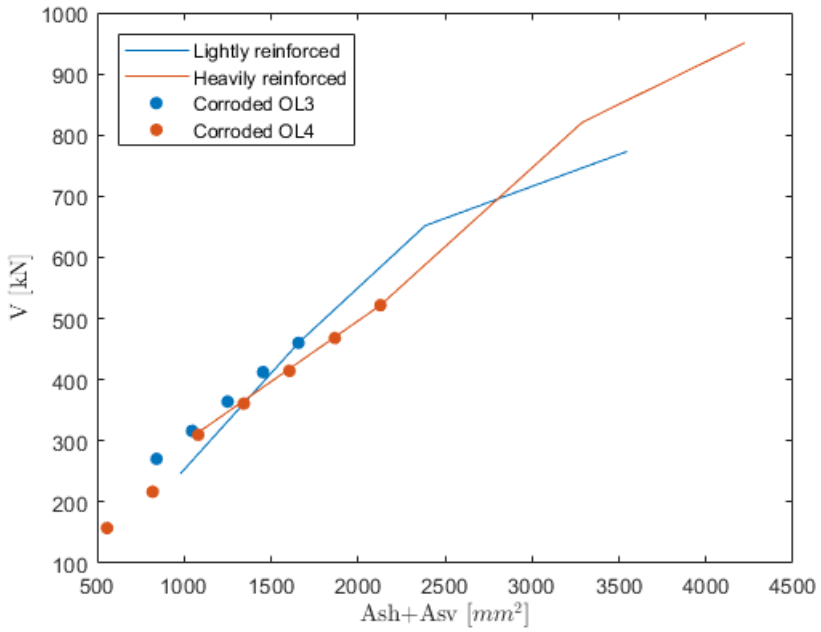

Figure 5.12: Resistance as a function of the amount of reinforcement evaluated without bond reduction and with the same reduction of section as the reduction of yield strength

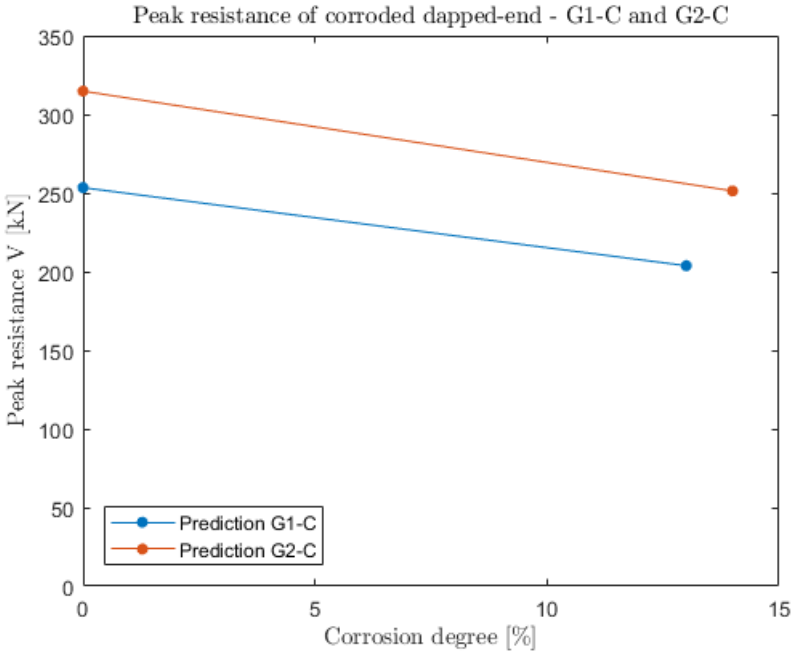

Figure 5.13: Effect of reinforcement amount - specimens G1-C and G2-C [18]

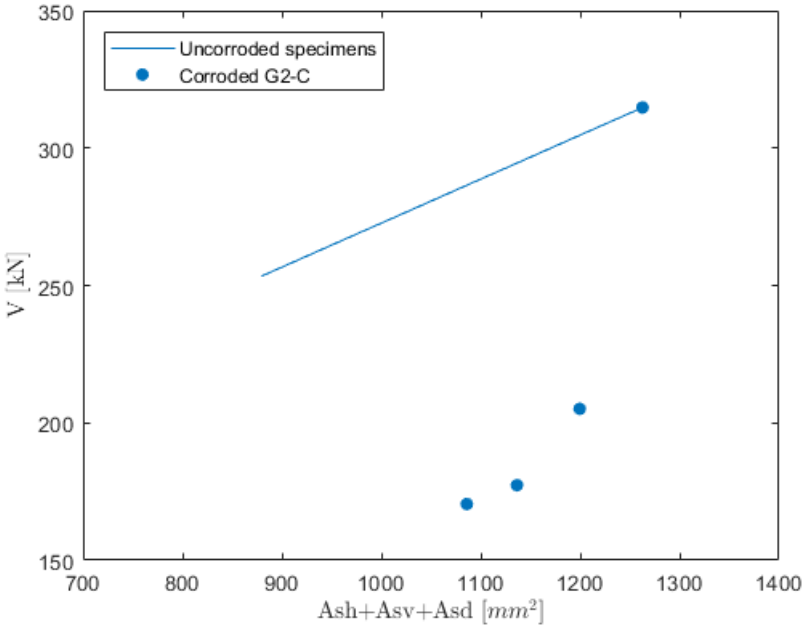

Figure 5.14: Resistance of the dapped-end as a function of the reinforcement amount - specimen G2-C

Chapter 6

Conclusion

This work presented the modelling of the effects of corrosion on the behavior of dapped-end connections. The following conclusions can be drawn.

- Several models are proposed to estimate the effect of corrosion on reinforcing bars. As they are empirical, it is important to choose a suitable model, based on a situation similar to the one being studied, in order to obtain satisfying results.
- The results of the proposed model are fairly close to those of experiments for models G1-C and G2-C, but rather far from the expected results for NS-LR. To conclude on the validity of this model, it should be compared with a larger number of tests than what is currently available in the literature.
- Corroded dapped-ends behave in the same way as lightly reinforced dapped-ends regarding the opening of cracks. Corroded bars are more brittle but the overall behavior of corroded dapped-end connections is more ductile.
- Estimating the corrosion level of bars by assuming the same loss of bar diameter for all bars gives similar results to those obtained with mean corrosion degree. Mean corrosion is a good substitute to the real corrosion degree as the predictions are safer while being close to the more accurate corrosion level.
- The resistance of more heavily reinforced half-joints decreases slightly more due to corrosion than for less reinforced dapped-end connections.
- The area of reinforcement is not modified in the model but the results show that the decrease of resistance due to corrosion follows the same trend as the decrease of resistance observed between uncorroded specimens with varying reinforcement amount.

To improve the present model and our understanding of the complex subject of corroded dapped-end connections, more experiments need to be carried out on these connections, ideally on naturally corroded specimens in service. To make the model more accurate, dapped-end pitting corrosion should also be modeled only in the nib. Finally, it would be interesting to be able to link the environment surrounding the half-joints to the degree of corrosion, so as to be able to predict the latter.

Bibliography

[1] Abdullah A. Almusallam et al. "Effect of reinforcement corrosion on bond strength". In: *Construction and Building Materials* 10.2 (Mar. 1996), pp. 123–129. DOI: 10.1016/0950-0618(95)00077-1.

[2] Abdullah A. Almusallam et al. "Effect of reinforcement corrosion on bond strength". In: *Construction and Building Materials* 10.2 (Mar. 1, 1996), pp. 123–129. DOI: 10.1016/0950-0618(95)00077-1.

[3] L. Amleh and S. Mirza. "Corrosion influence on bond between steel and concrete". In: *ACI Structural Journal* 96.3 (May 1999).

[4] Charis A. Apostolopoulos, Sotiris Demis, and Vagelis G. Papadakis. "Chloride-induced corrosion of steel reinforcement – Mechanical performance and pit depth analysis". In: *Construction and Building Materials*. 25th Anniversary Session for ACI 228 – Building on the Past for the Future of NDT of Concrete 38 (Jan. 1, 2013), pp. 139–146. DOI: 10.1016/j.conbuildmat.2012.07.087.

[5] YuBun Auyeung, P. Balaguru, and Lan Chung. "Bond Behavior of Corroded Reinforcement Bars". In: *MJ* 97.2 (Mar. 1, 2000), pp. 214–220. DOI: 10.14359/826.

[6] Kapilesh Bhargava et al. "Corrosion-induced bond strength degradation in reinforced concrete—Analytical and empirical models". In: *Nuclear Engineering and Design* 237.11 (June 1, 2007), pp. 1140–1157. DOI: 10.1016/j.nucengdes.2007.01.010.

[7] Kapilesh Bhargava et al. "Suggested Empirical Models for Corrosion-Induced Bond Degradation in Reinforced Concrete". In: *Journal of Structural Engineering* 134.2 (Feb. 1, 2008). Publisher: American Society of Civil Engineers, pp. 221–230. DOI: 10.1061/(ASCE)0733-9445(2008)134:2(221).

[8] J. G. Cabrera. "Deterioration of concrete due to reinforcement steel corrosion". In: *Cement and Concrete Composites* 18.1 (Jan. 1, 1996), pp. 47–59. DOI: 10.1016/0958-9465(95)00043-7.

[9] J. Cairns and R. B. Abdullah. "Bond strength of black and epoxy-coated reinforcement - A theoretical approach". In: *ACI Materials Journal* 93.4 (July 1996).

[10] J. Cairns et al. "Mechanical properties of corrosion-damaged reinforcement". In: *ACI Materials Journal* 102 (July 1, 2005), pp. 256–264.

[11] Giuseppe Campione et al. "Degraded Gerber Saddles in RC Bridges". In: *Journal of Performance of Constructed Facilities* 37.2 (Apr. 1, 2023). Publisher: American Society of Civil Engineers, p. 04022083. DOI: 10.1061/JPCFEV.CFENG-4016.

[12] M. P. Collins. "Towards a rational theory for RC members in shear". In: *Journal of the Structural Division* 104.4 (Apr. 1978).

[13] Dario Coronelli. "Corrosion cracking and bond strength modeling for corroded bars in reinforced concrete". In: *ACI Structural Journal* 99 (May 1, 2002), pp. 267–276.

[14] P. Desnerck, J. M. Lees, and C. Morley. "Impact of material deterioration on the strength of reinforced concrete half-joint structures". In: (2015). Publisher: International Association for Bridge and Structural Engineering (IABSE).

[15] Pieter Desnerck, Janet M Lees, and Chris Morley. "Assessment of reinforced concrete half-joint structures : dealing with deterioration". In: (2014).

[16] Pieter Desnerck, Janet M. Lees, and Chris T. Morley. "The effect of local reinforcing bar reductions and anchorage zone cracking on the load capacity of RC half-joints". In: *Engineering Structures* 152 (Dec. 2017), pp. 865–877. DOI: 10.1016/j.engstruct.2017.09.021.

[17] Pieter Desnerck, Janet M. Lees, and Chris T. Morley. "Strut-and-tie models for deteriorated reinforced concrete half-joints". In: *Engineering Structures* 161 (Apr. 2018), pp. 41–54. DOI: 10.1016/j.engstruct.2018.01.013.

[18] Fabio Di Carlo et al. "Experimental evaluation of the corrosion influence on the structural response of Gerber half-joints". In: *Engineering Structures* 285 (June 2023), p. 116052. DOI: 10.1016/j.engstruct.2023.116052.

[19] Congqi Fang. "Corrosion influence on bond in reinforced concrete". In: *Cement and Concrete Research - CEM CONCR RES* 34 (May 1, 2004). DOI: 10.1016/S0008-8846(04)00160-7.

[20] J. A. González et al. "Some questions on the corrosion of steel in concrete—Part I: when, how and how much steel corrodes". In: *Mat. Struct.* 29.1 (Jan. 1, 1996), pp. 40–46. DOI: 10.1007/BF02486005.

[21] Stefania Imperatore, Zila Rinaldi, and Carlo Drago. "Degradation relationships for the mechanical properties of corroded steel rebars". In: *Construction and Building Materials* 148 (Sept. 2017), pp. 219–230. DOI: 10.1016/j.conbuildmat.2017.04.209.

[22] Han-Seung Lee, Takafumi Noguchi, and Fuminori Tomosawa. "Evaluation of the bond properties between concrete and reinforcement as a function of the degree of reinforcement corrosion". In: *Cement and Concrete Research* 32 (Aug. 1, 2002), pp. 1313–1318. DOI: 10.1016/S0008-8846(02)00783-4.

[23] C. Q. Li, S. T. Yang, and M. Saafi. "Numerical Simulation of Behavior of Reinforced Concrete Structures considering Corrosion Effects on Bonding". In: *Journal of Structural Engineering* 140.12 (Dec. 1, 2014). Publisher: American Society of Civil Engineers, p. 04014092. DOI: 10.1061/(ASCE)ST.1943-541X.0001021.

[24] Karin Lundgren. "Modelling the effect of corrosion on bond in reinforced concrete". In: *Magazine of Concrete Research* 54.3 (June 2002). Publisher: ICE Publishing, pp. 165–173. DOI: 10.1680/macr.2002.54.3.165.

[25] S. Morinaga. "Remaining Life of Reinforced Concrete Structures after Corrosion Cracking". In: *Durability of Building Materials & Components 7 vol.1*. Num Pages: 10. Routledge, 2004. ISBN: 978-1-315-02502-5.

[26] Adam Neville. "Chloride attack of reinforced concrete: an overview". In: *Materials and Structures* 28.2 (Mar. 1, 1995), pp. 63–70. DOI: 10.1007/BF02473172.

[27] Yu-Chen Ou, Yudas Tadeus Teddy Susanto, and Hwasung Roh. "Tensile behavior of naturally and artificially corroded steel bars". In: *Construction and Building Materials* 103 (Jan. 30, 2016), pp. 93–104. DOI: 10.1016/j.conbuildmat.2015.10.075.

[28] S. Popovics. "Numerical approach to the complete stress-strain curve of concrete". In: *Cement and Concrete Research* 3.5 (Sept. 1973).

[29] Chathura Rajapakse. "Behaviour and Modelling of Reinforced Concrete Dapped-End Connections". In: (Feb. 2023). Publisher: ULiège - University of Liège [BE] [Faculty of Applied Sciences], Liège, Belgium.

[30] Chathura Rajapakse, Hervé Degée, and Boyan Mihaylov. "Assessment of Failure along Re-Entrant Corner Cracks in Existing RC Dapped-End Connections". In: *Structural Engineering International* 31.2 (Apr. 3, 2021). Publisher: Taylor & Francis _eprint: https://doi.org/10.1080/10168664.2021.1878975, pp. 216–226. DOI: 10.1080/10168664.2021.1878975.

[31] Chathura Rajapakse, Hervé Degée, and Boyan Mihaylov. "Investigation of shear and flexural failures of dapped-end connections with orthogonal reinforcement". In: *Engineering Structures* 260 (June 2022), p. 114233. DOI: 10.1016/j.engstruct.2022.114233.

[32] J. Rodriguez, Lara Marie Ortega, and J. Casal. "Corrosion of reinforcing bars and service life of reinforced concrete structures: Corrosion and bond deterioration". In: *International Conference on Concrete Across Borders* 2 (Jan. 1, 1994), pp. 315–326.

[33] Marco Martino Rosso et al. "Corrosion effects on the capacity and ductility of concrete half-joint bridges". In: *Construction and Building Materials* 360 (Dec. 19, 2022), p. 129555. DOI: 10.1016/j.conbuildmat.2022.129555.

[34] Viktor Sigrist. *Zum Verformungsvermögen von Stahlbetonträgern*. Artwork Size: 159 S. Medium: application/pdf. ETH Zurich, 1995, 159 S. DOI: 10.3929/ETHZ-A-001492371.

[35] G. J. Al-Sulaimani et al. "Influence of Corrosion and Cracking on Bond Behavior and Strength of Reinforced Concrete Members". In: *SJ* 87.2 (Mar. 1, 1990), pp. 220–231. DOI: 10.14359/2732.